Calspan

Technical Report

(12)

Calspan

THE CAPABILITY OF THE T-2 AIRCRAFT AS A HIGH ANGLE-OF-ATTACK IN-FLIGHT SIMULATOR

P. Motyka

Calspan Report No. AK-5759-F-1

Prepared for:

NAVAL AIR DEVELOPMENT CENTER
Warminster, Pennsylvania 18974

December 1975
Contract No. N62269-75-C-0388
Final Report

Calspan Corporation
Buffalo, New York 14221

UNCLASSIFIED

SECURITY CLASSIFICATION OF THIS PAGE (When Data Entered)

REPORT DOCUMENTATION PAGE

READ INSTRUCTIONS BEFORE COMPLETING FORM

1. REPORT NUMBER	2. GOVT ACCESSION NO. / 3. RECIPIENT'S CATALOG NUMBER
4. TITLE (and Subtitle): The Capability of the T-2 Aircraft as a High Angle-of-Attack In-Flight Simulator,	TYPE OF REPORT & PERIOD COVERED: FINAL
	6. PERFORMING ORG. REPORT NUMBER: AK-5759-F-1
7. AUTHOR(s): Paul R. Motyka	8. CONTRACT OR GRANT NUMBER(s): N62269-75-C-0388
9. PERFORMING ORGANIZATION NAME AND ADDRESS: Calspan Corporation, P.O.Box 235, Buffalo, New York 14221	10. PROGRAM ELEMENT, PROJECT, TASK AREA & WORK UNIT NUMBERS
11. CONTROLLING OFFICE NAME AND ADDRESS: Naval Air Development Center, Warminster, Pennsylvania 18974	12. REPORT DATE: Dec 1975 / 13. NUMBER OF PAGES: 64
14. MONITORING AGENCY NAME & ADDRESS (if different from Controlling Office)	15. SECURITY CLASS. (of this report): Unclassified / 15a. DECLASSIFICATION/DOWNGRADING SCHEDULE

16. DISTRIBUTION STATEMENT (of this Report)

DISTRIBUTION STATEMENT A
Approved for public release;
Distribution Unlimited

17. DISTRIBUTION STATEMENT (of the abstract entered in Block 20, if different from Report)

18. SUPPLEMENTARY NOTES

19. KEY WORDS (Continue on reverse side if necessary and identify by block number)

In-Flight Simulation
Variable Stability Airplane
High Angle-of-Attack Simulator
T-2 Airplane

20. ABSTRACT (Continue on reverse side if necessary and identify by block number)

This report documents the results of a conceptual control system study undertaken to determine the feasibility of employing a T-2, configured for variable stability operation, as a high angle-of-attack simulator and ascertain the envelope over which a valid simulation can be obtained.

OVER

DD FORM 1 JAN 73 1473 EDITION OF 1 NOV 65 IS OBSOLETE

Unclassified

SECURITY CLASSIFICATION OF THIS PAGE (When Data Entered)

A model-following control system is defined that forces the T-2 to duplicate the motions of departing aircraft which exhibit characteristics of airplanes in the Navy inventory.

The quality of simulation is excellent within an envelope defined by 15 deg in incremental angle of attack and ± 15 deg in sideslip. A faithful reproduction of the predeparture and initial sudden departure motions of the model aircraft is obtained within this envelope and would allow for good training transfer in the difficult-to-train incipient departure region of flight. Techniques for modifying the model aircraft responses to increase the simulation capability of the variable stability T-2 are investigated. Several promising methods for doing this are developed and evaluated.

ABSTRACT

This report documents the results of a conceptual control system study undertaken to determine the feasibility of employing a T-2, configured for variable stability operation, as a high angle-of-attack simulator and ascertain the envelope over which a valid simulation can be obtained.

A model-following control system is defined that forces the T-2 to duplicate the motions of departing aircraft which exhibit characteristics of airplanes in the Navy inventory.

The quality of simulation is excellent within an envelope defined by 15^{o} in incremental angle of attack and $\pm 15^{o}$ in sideslip. A faithful reproduction of the predeparture and initial sudden departure motions of the model aircraft is obtained within this envelope and would allow for good training transfer in the difficult-to-train incipient departure region of flight. Techniques for modifying the model aircraft responses to increase the simulation capability of the variable stability T-2 are investigated. Several promising methods for doing this are developed and evaluated.

FOREWORD

This report was prepared by the Calspan Corporation, Buffalo, New York for the Naval Air Development Center, Warminster, Pennsylvania. The work was performed under Contract N62269-75-C-0388, entitled "Feasibility Study of Using a T-2 Aircraft to Simulate High Angle-of-Attack Behavior". The Naval Air Development Center project engineer was Mr. A. Piranian under the technical supervision of Mr. C. Mazza. The project engineer for Calspan was Dr. P. Motyka who was responsible for most of the technical content of this report. Mr. R. Radford developed the analytic model of the T-2 aircraft. The computer programming effort was the responsibility of Mr. C. Mesiah and Mr. T. Diegelman. Miss F. Scribner prepared this report for publication, Mrs. M. Ford and Miss D. Kantorski typed the manuscript. Many important and useful suggestions were made by Mr. E. Rynaski and Mr. R. Wasserman. The author wishes to thank all of these people for their help and suggestions during the course of this program.

This report was submitted by the author in December 1975 and is being published as Calspan Report No. AK-5759-F-1.

TABLE OF CONTENTS

LIST OF FIGURES

LIST OF SYMBOLS

A, B, C	General Coefficients of a Cubic Equation
b	Reference Span of Wing, feet
$\bar{c}$	Mean Aerodynamic Chord, feet
ΔCG	Difference in Actual c.g. Position and c.g. position at which Aerodynamics are Defined, percent of $\bar{c}$
CG_{POS}	Position of Center of Gravity, percent of $\bar{c}$
C_D	Drag Coefficient
C_L	Lift Coefficient
C_{L_i}	$\partial C_L / \partial i$, $i = \alpha, \delta_z$, deg^{-1}
C_ℓ	Rolling Moment Coefficient
C_m	Pitching Moment Coefficient
C_n	Yawing Moment Coefficient
$C_{n_{\delta_r}}$	$\partial C_n / \partial \delta_r$, deg^{-1}
C_x	Longitudinal Body Axis Force Coefficient
C_y	Lateral Body Axis Force Coefficient
C_{y_β}	$\partial C_y / \partial \beta$, deg^{-1}
C_z	Normal Body Axis Force Coefficient
f	Polynomial Functional Relationship
F	Force
g	Gravitational Constant, 32.2 ft/sec^2
h	Absolute Altitude, feet
i_m	Angle-of-Attack Mismatch, deg
I	Matrix of Inertias
I_x, I_y, I_z	Moments of Inertia About x, y, z Body Axes, slug-ft^2

LIST OF SYMBOLS

I_{xz}	Product of Inertia About x, z Body Axes, slug-ft^2
K_i	Scaling Constant, $i = \alpha, \beta, V$
$K_{L.G.}$	1, Landing Gear Down 0, Landing Gear Up
ℓ_x, ℓ_y, ℓ_z	Distances Along x, y, z Body Axes, feet
M	Moment
Mn	Mach Number
m	Mass of Airplane
n_x, n_y, n_z	Longitudinal, Lateral and Normal Accelerometer Signals, g's
p, q, r	Roll, Pitch, Yaw Rates, deg/sec
$\bar{q}$	Dynamic Pressure, lb/ft^2
s	Laplace Operator, sec^{-1}
t	Time, sec
T	Total Thrust of Airplane, lbs.
T_c'	Normalized Thrust = $T/\bar{q}S$
$\mathcal{T}$	Transformation Matrix
u, v, w	Velocity Along x, y, z Body Axes, ft/sec
V	True Airspeed of Center of Gravity of Airplane, ft/sec
$(\dot{})$	First Derivative With Respect to Time
α	Total Angle of Attack, deg
β	Total Angle of Sideslip, deg
δ	General Control Deflection
δ_a	Aileron Surface Deflection, Positive for TE Right Surface Down, deg
δ_e	Elevator Surface Deflection, Positive TED, deg

LIST OF SYMBOLS

δ_r	Rudder Surface Deflection, Positive TEL, deg
δ_y	Side-Force Surface Deflection, Positive TEL, deg
δ_z	Direct Lift Surface Deflection, Positive TED, deg
Δ	Incremental Value of Variable
γ	Flight Path Angle, deg
ρ	Air Density, slug/ft^2
ϕ	Bank Angle, deg
θ	Pitch Angle, deg
ψ	Heading Angle, deg
τ	Time Constant, sec
ω	Vector of p, q, r
ω_x	Matrix of p, q, r

Subscripts

Aero	Aerodynamic
C	Command Signal
GRAV	Gravity
m	Model
n	Negative
o	Initial
P	Positive
t	Trim
U.T.	Untrimmed

LIST OF SYMBOLS

Subscripts

T	Transformed
T-2	T-2 Airplane

Superscripts

-1	Inverse
—	Linear Estimate

Section I

INTRODUCTION

The continuing loss of a significant number of military aircraft due to lack of control in high angle-of-attack flight requires that a concentrated effort be undertaken to increase technical knowledge in the stall/departure/spin regime. A promising means of safely and effectively investigating this area of dangerous flight is through the use of variable stability aircraft. An aircraft that simulates the fringe controllability flight regime of another airplane totally within the safe, controllable flight range of the simulator airplane would be useful not only as a research tool but as a trainer as well, providing stall/departure training to fleet pilots.

This report describes the results of a feasibility and conceptual control system design study undertaken by the Calspan Corporation for the Naval Air Development Center to determine the range of high angle-of-attack simulation capability of the T-2 aircraft configured for variable stability operation. The present study is a direct outgrowth and extension of a previous one (Reference 1.1) which investigated the potential usefulness of a variable stability T-2 for training applications. It was concluded in this initial study that the T-2 "is an outstanding aircraft for conversion to a variable stability airplane of a quality and wide-range of capability never before contemplated for this type of aircraft conversion". The study was concerned with methods of adding direct-force control to the basic T-2, variable stability system space and power requirements, estimates of the ability of the variable stability aircraft to simulate the dynamic motions of other aircraft and the complexity of the computational system required to do this.

1.1 Rynaski, E., et.al., "Preliminary Design and Training Application Analysis of a YT-2B In-Flight Simulator, Calspan Report No. AK-5362-F-1, January 1974.

The initial study (Reference 1.1) is used as a reference point to investigate the high angle-of-attack simulation capability of a variable stability T-2. The intent of the study described in this report is to determine if a variable stability T-2 can be used as a stall/departure simulator and ascertain its simulation envelope and the degree to which it will be able to match the forces and moments of departing aircraft. These items are investigated using a digital simulation of a T-2 variable stability system and analysis of the simulation results. A conceptual model-following control system is developed to allow the T-2 to duplicate the motions of the model aircraft which exhibit characteristics of existing Navy aircraft, such as the F-4, F-14 and A-7. However, a determination of the degree to which the T-2 can simulate each of these particular aircraft is not the major goal of this study. It has been assumed for this study that the T-2 is to operate at less than its stall angle of attack within its controllable flight regime. Also, no detailed consideration is given to the effects of the maneuvers performed by the T-2 on its structural integrity; however, the maneuvers examined showed no significant problems. Methods are also investigated for altering the angle of attack and sideslip of the model aircraft to provide more simulation flexibility and capability. Three techniques for accomplishing this are discussed in this study involving the scaling and filtering of these variables.

Section II contains a discussion of the technical approach used in this study. A block diagram of the model-following system which evolved is presented and the function of each of the components is discussed. The data incorporated into each of these components is presented in the appendices.

Section III contains results, in the form of time histories, obtained to determine the simulation envelope of the variable stability T-2. Model and T-2 responses are overplotted to give a direct visual display quality of model following. Control deflection time histories are also presented. A discussion of the results is included.

Transformations of the angle of attack and sideslip of the model aircraft, designed to provide more simulation flexibility, are presented and discussed in Section IV. Time history plots are included to show the effect

of employing these transformations. The report ends with the conclusions drawn from this study effort which are contained in Section V. Several areas where additional study should be initiated are also discussed.

Section II
TECHNICAL APPROACH AND DATA

The technical approach used to determine the feasibility of employing the T-2 as a high angle-of-attack simulator is explained in this section. A block diagram of the model-following system developed for this purpose is presented and the function of each of the components of the system discussed. The detailed equations programmed on the computer for each of these components are presented in the appendices.

2.1 Technical Approach

The feasibility of using the T-2 as a high angle-of-attack simulator of current Navy fighter/attack aircraft was verified. A model-following control law was developed and implemented in an existing Calspan digital computer program designed to simulate the operation of variable stability aircraft (Reference 2.1). This digital computer program solves the six degree-of-freedom, nonlinear, rigid body equations of motion for both the model and simulator aircraft. The simulator aircraft control surface deflections are computed using a programmed model-following control law. Time histories of the model aircraft control surface deflections are inputs to the program. The ability to simulate the variable stability airplane actuators and atmospheric turbulence effects are also features of this program, although high performance actuators were assumed for all control surfaces and the throttle but gusts were not considered during the course of this particular study. The outputs of this program are the model and simulator aircraft trim conditions and printed and plotted time history responses and control deflections.

A block diagram of the model-following system which evolved during this program is shown in Figure 2.1. The components which make up this system are discussed below.

2.1 Mesiah, C., "DSTIFS - Digital Simulation of a Variable Stability Total In-Flight Simulator", Flight Research Memorandum No. 434, April 1970.

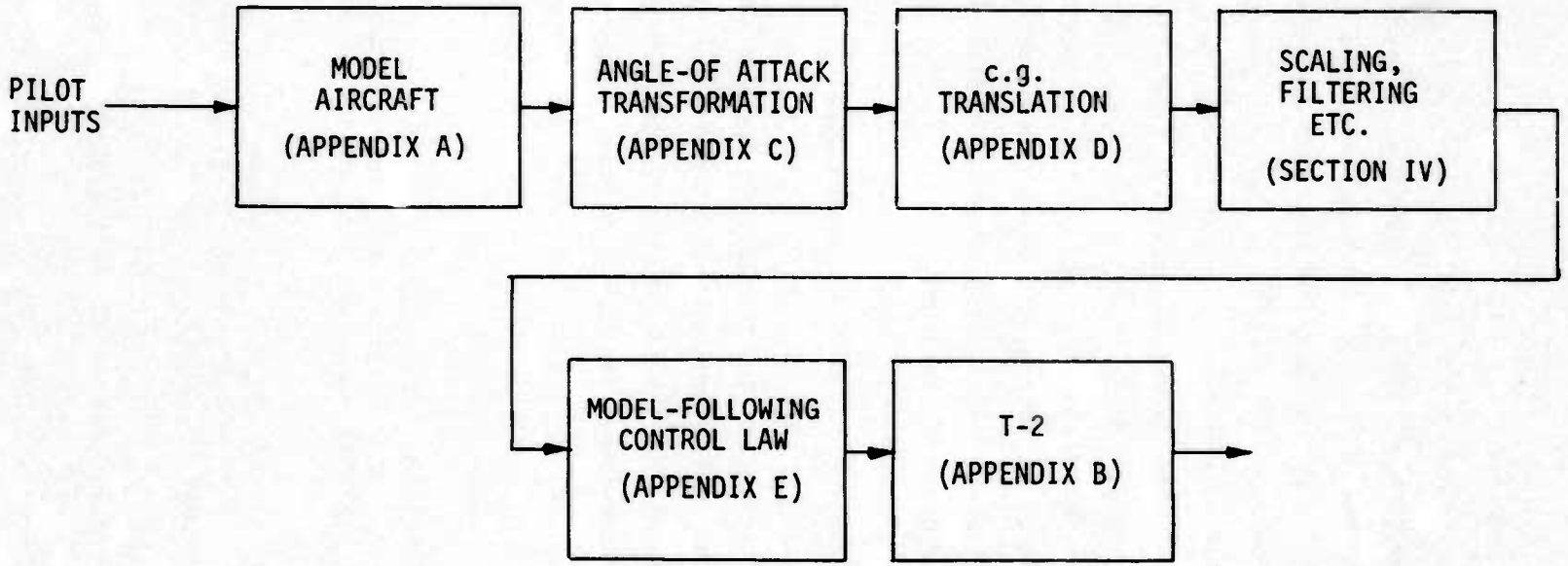

Figure 2.1 MODEL-FOLLOWING SYSTEM BLOCK DIAGRAM

2.2 Model Aircraft

The F-4 was selected as the model aircraft for the initial and major part of this study. The general body axis equations of motion of the model aircraft are given in Appendix A. The aerodynamics of the F-4 model were obtained from Reference 2.2 where they are presented as polynomial functions in three angles-of-attack regions; 0^{o}-15^{o}, 15^{o}-30^{o} and greater than 30^{o}. The equations for the forces and moments due to thrust are also given. A second model aircraft made use of the lateral-directional characteristics of the A-7 given in Reference 2.3 while retaining the longitudinal characteristics of the F-4 model. These characteristics were fit with polynomial functions in the same three angle-of-attack ranges as the F-4. A third model aircraft was developed from F-14 data presented in Reference 2.4 except that the lift and drag coefficients of the F-4 were retained.

2.3 T-2 Aircraft Equations of Motion and Aerodynamics

The T-2 equations have been modified to include side-force and direct-lift control to produce independent Y and Z forces. Reference 1.1 discusses the rationale for choosing these particular surfaces as well as their effectiveness in increasing the model-following capability of the T-2

2.2 Eulrich, B., Weingarten, N., "Identification and Correlation of the F-4E Stall/Post Stall Aerodynamic Stability and Control Characteristics From Existing Test Data", Calspan Report No. AK-5126-F-1, November 1973. (AFFDL-TR-73-125)

2.3 Chen, R., Newell, F., Schelhorn, A., "Development and Evaluation of an Automatic Departure Prevention System and Stall Inhibitor for Fighter Aircraft", Calspan Report No. AK-5112-F-1, April 1973. (AFFDL-TR-73-29)

2.4 Eney, J., "Moving Base Simulation of the F-14 Stall/Spin", NADC-73085-30, June 1973.

aircraft. Total In-Flight Simulator (TIFS) data was used to estimate the effectiveness of these control devices (Reference 2.8). It was not possible to estimate the effect of the side-force surfaces on the stability and control parameters of the variable stability T-2 at high angles of attack since no such data is available in this flight regime. For the purposes of this study the control surfaces of the T-2 are limited at the values indicated in Table 2.1.

The equations of motion of the T-2 programmed into the variable stability simulation program are the same as those of the model aircraft given in Appendix A. The T-2 aerodynamic data is given in Appendix B. These data were obtained from References 2.5, 2.6, 2.7 and 2.8.

TABLE 2.1

T-2 CONTROL SURFACE LIMITS

Control	Limit	Control	Limit
δ_a	$\pm 25^o$	δ_e	$+15, -27^o$
δ_r	$\pm 25^o$	T	0, 10,000 lb
δ_y	$\pm 21^o$	δ_z	$\pm 30^o$

2.5 Schuetz, A., Bailey, D., "Low Speed Wind Tunnel Investigation of a .09 Scale Navy Model T-2C Subsonic Jet Trainer Aircraft From -8 to +83 Degrees Angle of Attack", Report No. NADC-73259-30, December, 1973.

2.6 Schuetz, A., "Analysis of Variable Lift Curve Slope for a Proposed Variable-Stability NT-2B Airplane", Report No. NADC-AM-6958, November 1969

2.7 "Estimated Aerodynamic Characteristics Design of the T2J-1 Airplane", North American Aviation Columbus Division, Report No. NA-57H-580, January 1958.

2.8 Reynolds, P., et al, "Capability of the Total In-Flight Simulator (TIFS)", AFFDL-TR-72-39, July 1972.

2.4 Angle-of-Attack Transformation

The outputs of the model aircraft are programmed to undergo a constant angle-of-attack transformation or offset. This transformation is required since the T-2's stall angle of attack is about 16 degrees. The F-4, A-7 and F-14 aircraft used in this study departed at a substantially greater angle of attack.

The approach used in this study is to trim the aircraft to be simulated, or model, at a high angle of attack close to its departure boundary. The T-2 is trimmed at a small or even negative angle of attack. The angle-of-attack transformation is required to account for the differences in the angle of attack of the model and T-2. This provided the widest useful dynamic simulation range since it is desired to simulate only the high angle-of-attack operation of the model and the simulation envelope of the T-2 ranges from its trim angle of attack to its stall angle of attack. One of the consequences of employing this transformation is that the visual field of the simulation pilot differs statically by the angle-of-attack bias. The trim attitude of the T-2 is transformed by the angle-of-attack mismatch. A consideration of techniques such as the masking of the T-2's windows or alteration of the deck angle may be required so that the visual scene is the same as that for the model aircraft. However, this effect may not be important since airplanes with higher stall angles of attack usually have more down vision from the cockpit. This would make the T-2 pilot's view more nearly the same as the model aircraft.

The angle-of-attack transformation used in this study and its effect on the model aircraft variables is presented in Appendix C.

2.5 c.g. Translation

The next component of the model-following system involves a translation of the model responses from the model c.g. to the T-2 c.g. It is assumed that the pilots station of the model aircraft and the T-2 are

coincident so that the simulation pilot undergoes the same responses as if he were flying the model aircraft. This implies that the c.g. of the model aircraft and T-2 are not coincident because of physical differences in the two aircraft. A translation of the model responses from the model c.g. to the T-2 c.g. is required. Appendix D gives the appropriate equations.

2.6 Scaling, Filtering Transformations

The angle-of-attack transformation discussed previously accounted for differences in trim angle of attack between the model and T-2. However, the dynamic angle-of-attack range of the model may exceed that of the T-2. The same is true of the sideslip angle. Therefore, a variety of schemes such as the scaling of $\Delta\alpha_m$ and β_m and the washout filtering of these signals were tried to compress the α,β envelope of the model aircraft into that which the T-2 can simulate. These transformations and the results obtained using them are discussed in Section IV.

2.7 Model-Following Control Law

The model aircraft responses which have been transformed, translated, etc. are then fed into the model-following control law where the T-2 control surface deflections required to achieve the model responses are computed. The model-following control law was developed using theory presented in Reference 2.9 and consists of feedforward and feedback paths. Basically, the feedforward portion of the model-following control law is based upon the equations of motion of the T-2 vehicle. The model responses are the desired T-2 responses, and the equations are solved for the T-2 control deflections which achieve these responses. If the feedforward equations solved for the control deflections are exactly the same as those of the T-2, the model and T-2 responses will be identical as long as surface limits are not encountered or the capability of the T-2 exceeded. Feedback is not necessary for the

---

2.9 Motyka, P., "Variable Stability System Control Concepts For A Fighter In-Flight Simulator", Calspan Report No. IB-2895-F-1, December 1970.

matching of the T-2 and model responses if the T-2 is known exactly. It can then be used for any other desired purpose. For example, it can be used to reduce the sensitivity of the model-following system to T-2 parameter variations as it is on TIFS. Feedback of the T-2 responses is not considered in this study since the T-2 control deflections which result in the matching of the T-2 and departing model aircraft responses can be calculated solely from the feedforward portion of the control law.

The effectiveness of the postulated T-2 side-force surfaces is cubic in nature (Appendix B). This means that a cubic equation has to be solved in the model-following control law to obtain the T-2 side-force deflection which results in identical model and T-2 responses. It was determined that a much simpler model-following control law is obtained using a linearized estimate of the side-force surface effectiveness. The T-2 side-force surface deflection can then be obtained from a closed form expression rather than by iterative techniques as required if the cubic effectiveness is retained. As a result small errors in model following occur since the side-force equations of the T-2 and feedforward control law differ.

The control effectiveness nonlinearities were taken into account in the longitudinal model-following control law. Estimates of the control surface deflections were obtained using linearized effectiveness coefficients. These estimates were then refined by accounting for the nonlinear effectiveness. The final equations programmed for the model-following control law are given in Appendix E.

2.8 Equipment Considerations

It is felt that the model-following system discussed in this section can be implemented in an airborne digital computer. No unusual equipment is required for the system developed. The most complex portion will be the implementation and solution of the model equations of motion which must be

nonlinear and cover a large angle-of-attack range. The additional transformations and model-following control law solved to obtain the T-2's control deflections are straightforward. In fact, the additional use of feedback gains to lessen model-following errors may allow simplifications to be made in the control law. For example, the control nonlinearities in δ_y and δ_e or some of the minor terms in the equations may be eliminated with little or no deterioration in the quality of model following.

Section III

RESULTS

The results obtained during the course of this study are presented primarily in the form of time history plots. The state variables of the model and T-2 are overplotted to indicate the quality of model following. Control deflection time histories of both aircraft are also given. Results are presented for the F-4 model in the approach and clean configurations, the A-7 model in the clean configuration and the F-14 model in the clean configuration.

3.1 Model-Following Results, F-4 Model, Approach Configuration

Figure 3.1 shows responses of a T-2 model following a departing F-4 in the approach configuration. The F-4 is trimmed at α_t = 20.633°, V_t = 230 fps and h_t = 7400 ft with the gear down. A bias angle-of-attack mismatch of 16° has been introduced between the F-4 model and the T-2. The model responses shown in Figure 3.1 are those which have been modified by the angle-of-attack transformation which is presented in Appendix C, and a translation from the F-4 c.g. to the T-2 c.g. (Appendix D).

A δ_e ramp is applied to the F-4 to increase the angle of attack from its trim value. It is also necessary to use a very small lateral perturbation input to the F-4 of small amplitude to excite its lateral-directional modes and is needed strictly because a computer simulation ordinarily does not contain all the minor excitation present in a real aircraft. If this input is not employed the F-4 digital simulation will not diverge when its departure angle of attack is reached. This is due to the form of the lateral-directional aerodynamic equations used to define the F-4 model which contain no purely longitudinal effects and the fact that the F-4 is trimmed in level flight with all of the lateral-directional variables zero. In the latter case, coupling effects between the longitudinal and lateral-directional modes remain at zero since the lateral-directional variables remain at zero unless perturbed. In any event, the amplitude of the δ_a input is of such a small magnitude that it can be considered a disturbance input.

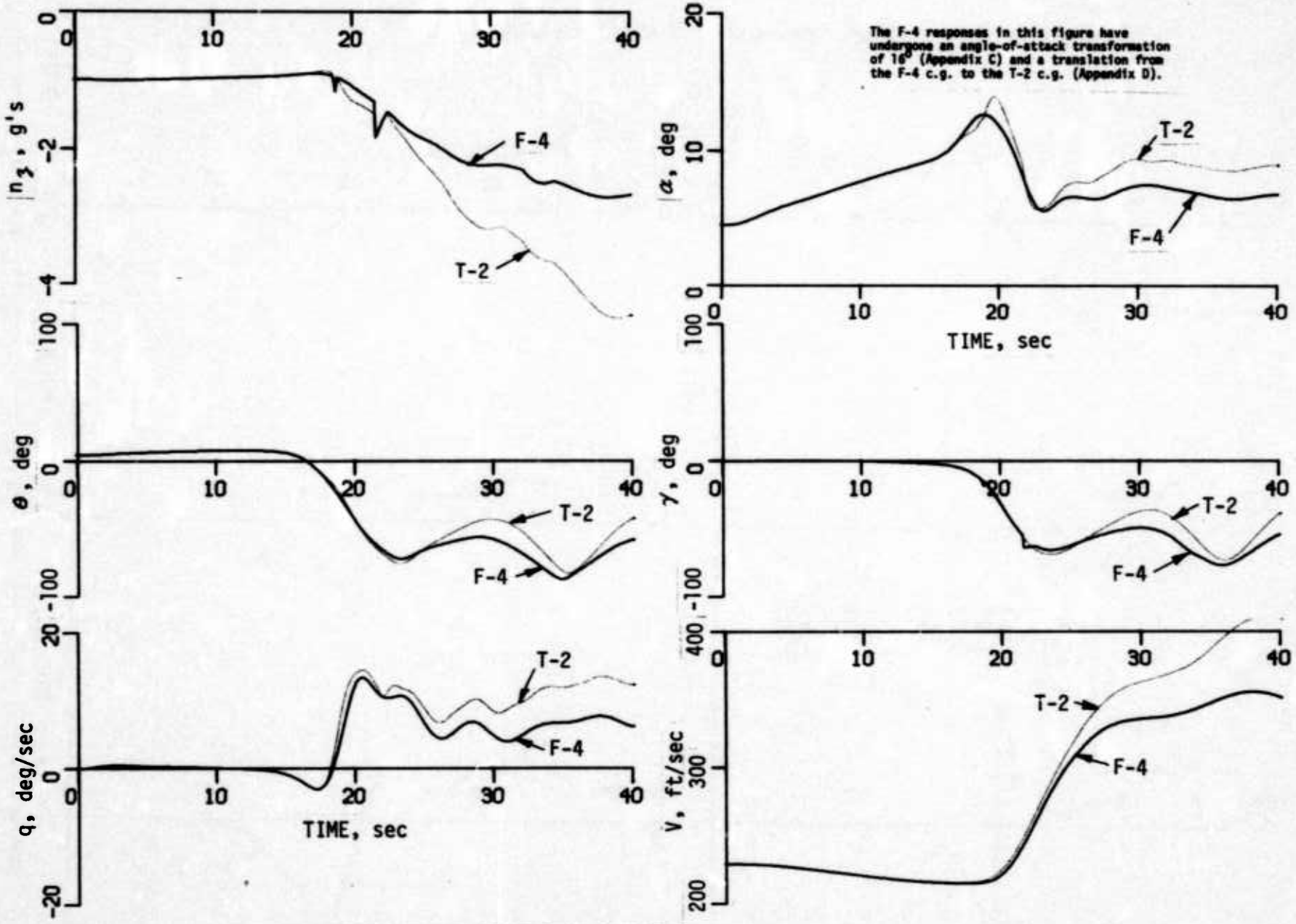

Figure 3.1 T-2 SIMULATION OF AN F-4 DEPARTURE, APPROACH CONFIGURATION

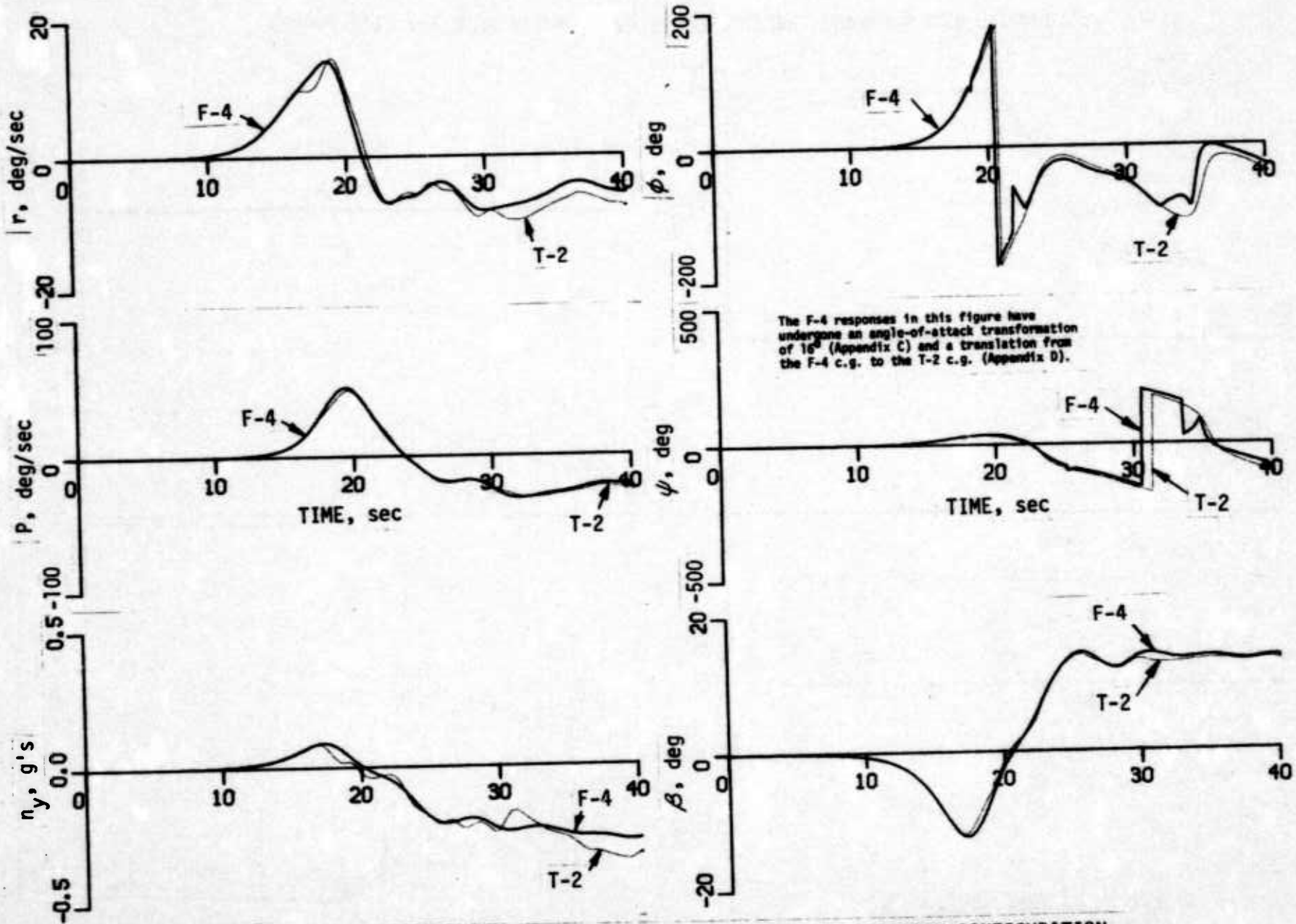

Figure 3.1 (cont'd) T-2 SIMULATION OF AN F-4 DEPARTURE, APPROACH CONFIGURATION

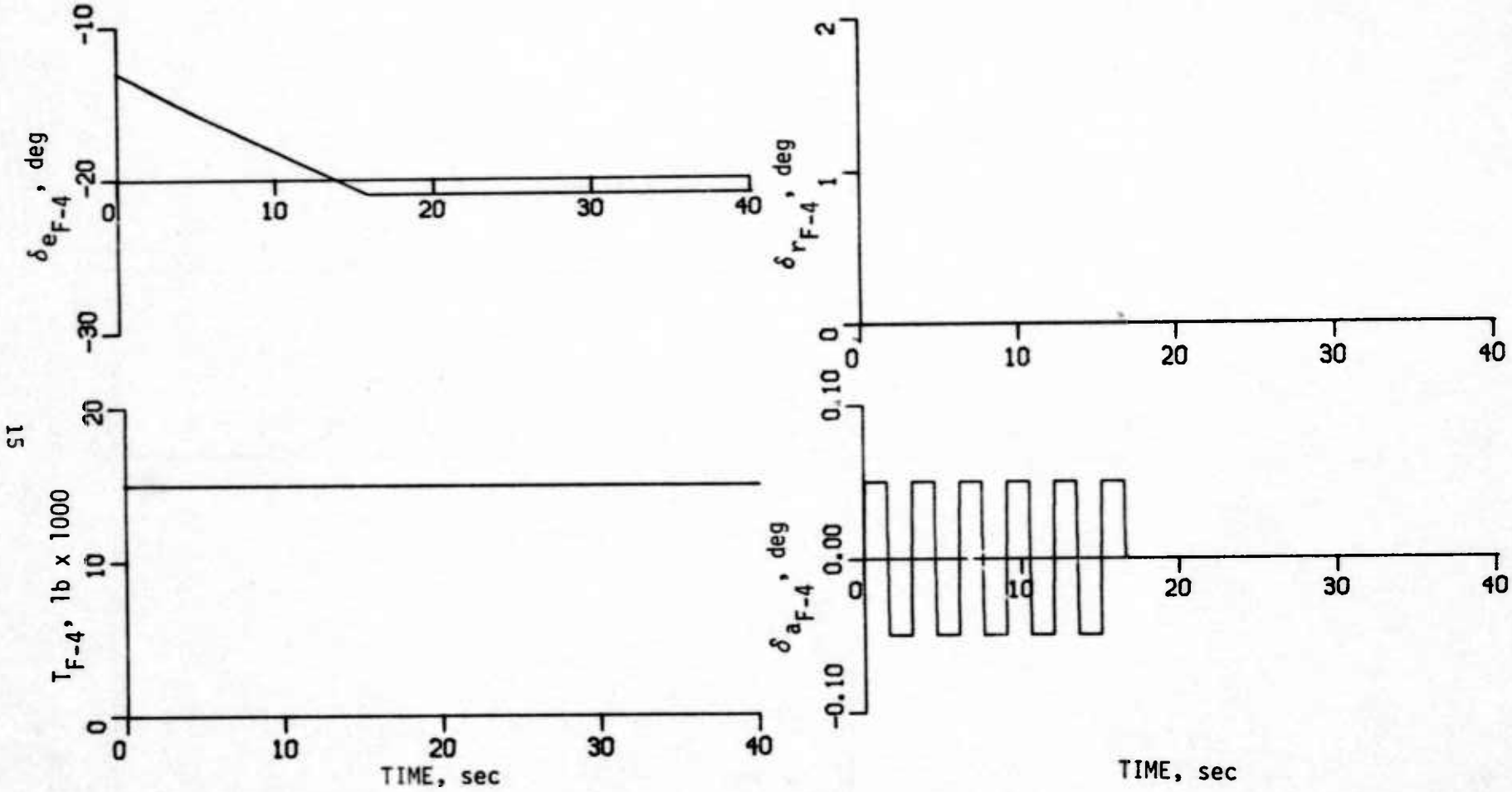

Figure 3.1 (cont'd) T-2 SIMULATION OF AN F-4 DEPARTURE, APPROACH CONFIGURATION

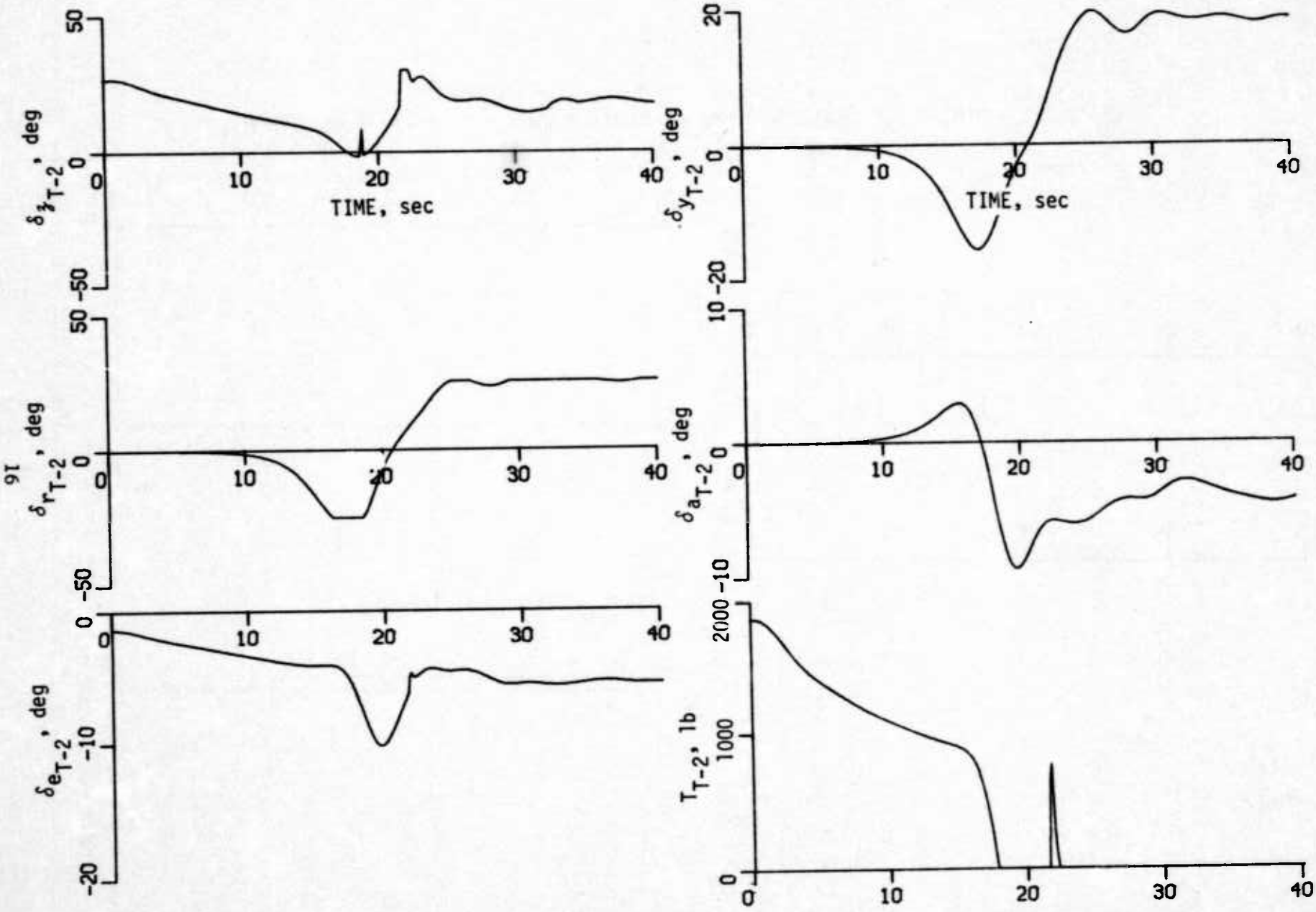

Figure 3.1 (concl'd) T-2 SIMULATION OF AN F-4 DEPARTURE, APPROACH CONFIGURATION

"Glitches" are present in some of the F-4 responses and occur because the model is transitioning from one angle-of-attack polynomial range to an adjacent one. The "glitches" also show up in the T-2 control deflections and responses. δ_z and T_{T-2} are examples. A discontinuity, which should not be there, is evident in each variable at about 21 sec into the trace because of this. The "glitch" is a digital simulation irregularity that would not, of course, be present in the real aircraft. From the standpoint of the actual operation of the T-2 it would be better to implement the model aircraft in table look-up form with an appropriate interpolation scheme. This approach would avoid major errors due to the fitting of the data and transients in the time history responses due to the transitioning from one angle-of-attack range to the adjacent one. In the actual T-2 it would be impractical to span the whole angle-of-attack region of interest with polynomials since they would have to be of extremely high order. Table look-up is the better method to use for this type of simulation.

In Figure 3.1 the angle of attack of the F-4 increases linearly with time for about the first 17 sec. of the time history. At this time the lateral-directional variables begin to show that the vehicle is in a state of incipient departure, and occurs when the F-4's angle of attack reaches $\approx$ 24 degrees and is first noticeable in β, p, r and n_y. The longitudinal variables q, θ, γ and n_z are then excited because of coupling effects between the lateral-directional and longitudinal modes. Eventually, the F-4 rolls over at 21 sec on the time history and enters a spin at about 30 sec on the time history.

With the exception of the angle-of-attack mismatch mentioned previously, Figure 3.1 shows that the T-2 can simulate the departure dynamic characteristics very well. The pitch attitude change of the T-2 matches that of the F-4 within a few degrees up to about 80° and the pitch rates are coincident within 2°/sec or less. The lateral-directional characteristics are matched even more closely, with differences between the F-4 and F-2 of a maximum of less than 2°/sec in p and r, .01 g in n_y and even less in attitude. Excellent simulation is possible through a complete 360° roll and spin. The maximum simulation error occurs in n_z, but this error is only about

.2g and at a time after the T-2 has done a complete 360° roll. Only the rudder saturates for a couple of seconds near a 90° roll angle, so the T-2 does have the force and moment generating power to accurately simulate the F-4 departure in the approach configuration of the F-4. After the F-4 has executed a 360° roll, the aircraft is assumed to be in more of a spin than departure condition, and the spin condition simulation is beyond the scope of this study or the existing capability of the T-2.

After 20 sec into the time history, the thrust of the T-2 goes to zero and quality of the model following of the longitudinal variables then deteriorate (after the departure) because the T-2 does not have enough drag. A T-2 configured as a spin simulator would need additional drag producing devices. A similar conclusion was reached in the preliminary Y-2 study effort (Reference 1.1). The thrust required time history of Figure 3.1 defines the drag requirements for accurate simulation. From this time history the adequacy of drag producing devices such as speed brakes can be defined. If necessary, new or additional drag devices can be designed.

The aerodynamic control surfaces of the T-2 have adequate power to allow the T-2 to model follow the F-4 during this maneuver. The rudder limits momentarily at about 15 sec into the time history which causes the r and n_y following to deteriorate very slightly. The rudder is also on the verge of limiting when the F-4 is in the spin and this causes additional model-following errors in r and n_y . δ_z also reaches its positive limit momentarily at about 21 sec into the time history but the effect of this is not noticeable.

3.2 Model-Following Results, F-4 Model, Clean Configuration

The F-4 model in the clean configuration was used next in the study. Figure 3.2 contains the time histories. The model is trimmed at α_t = 20.095°, V_t = 446 fps and h_t = 10,000 ft. An angle-of-attack mismatch of 23.5° is introduced between the model and T-2 so that the direct lift control surfaces are trimmed near their positive lower limit allowing the largest maneuver range possible. The T-2 trim angle of attack is -3.405°.

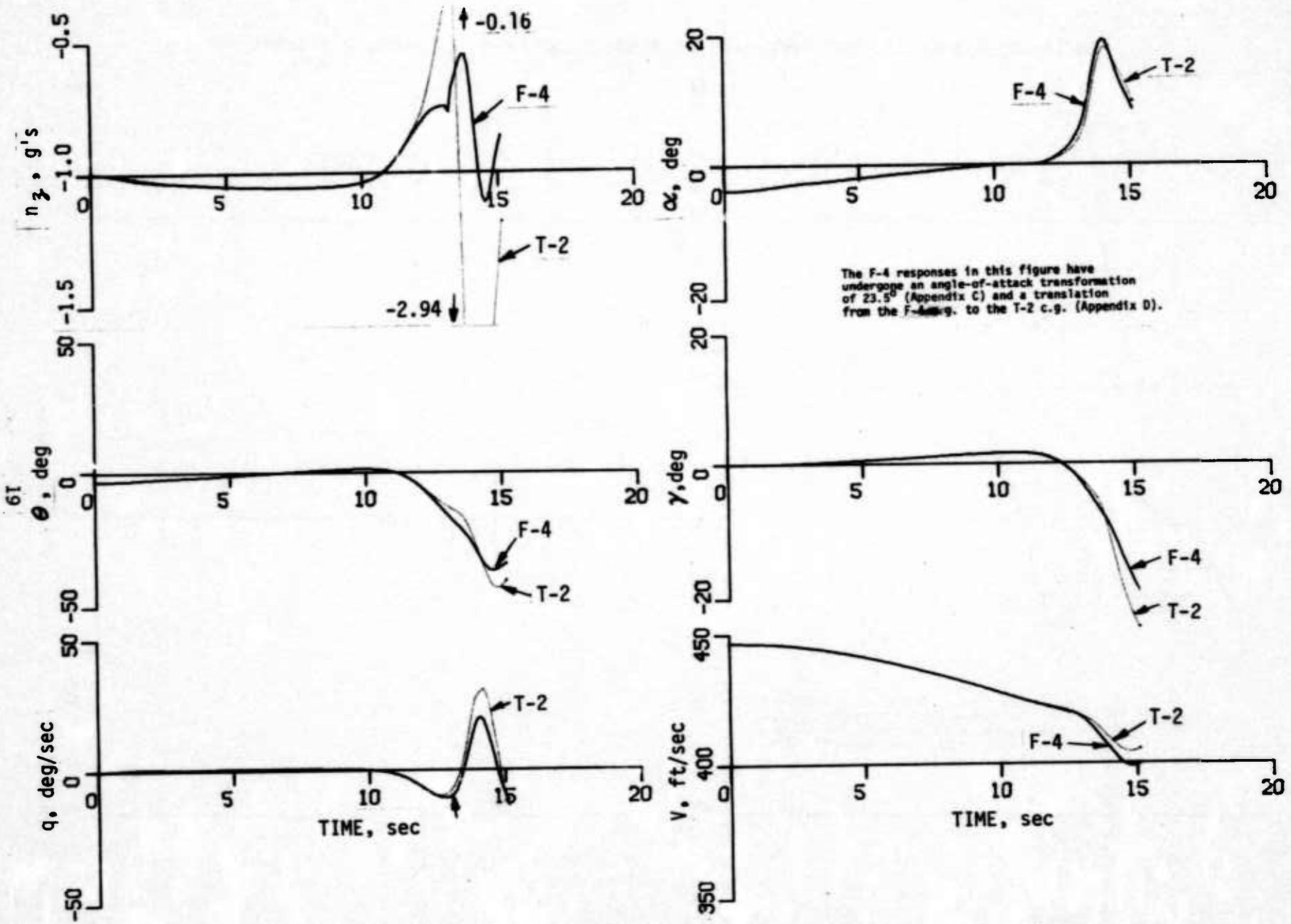

Figure 3.2 T-2 SIMULATION OF AN F-4 DEPARTURE, CLEAN CONFIGURATION

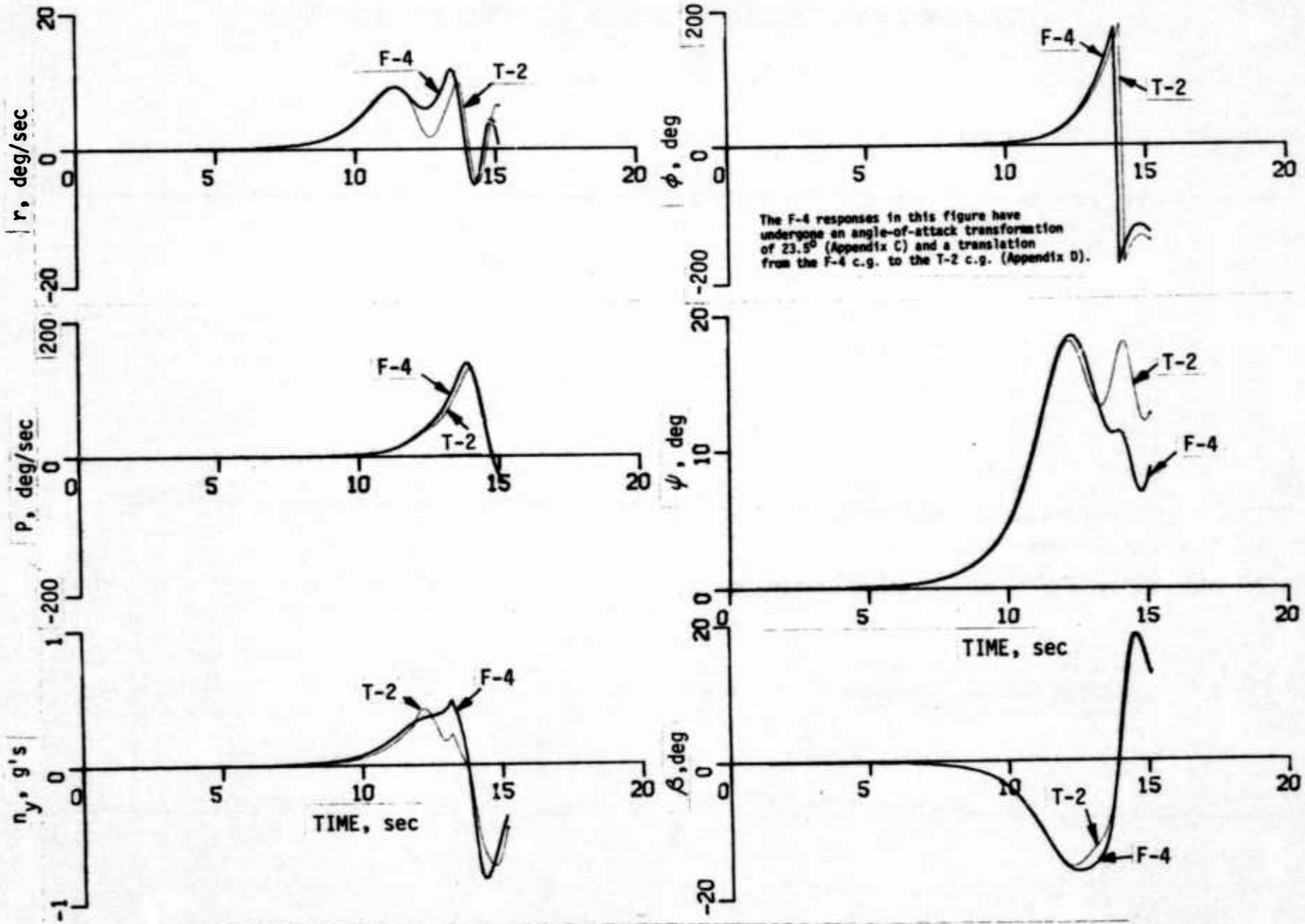

Figure 3.2 (cont'd) T-2 SIMULATION OF AN F-4 DEPARTURE, CLEAN CONFIGURATION

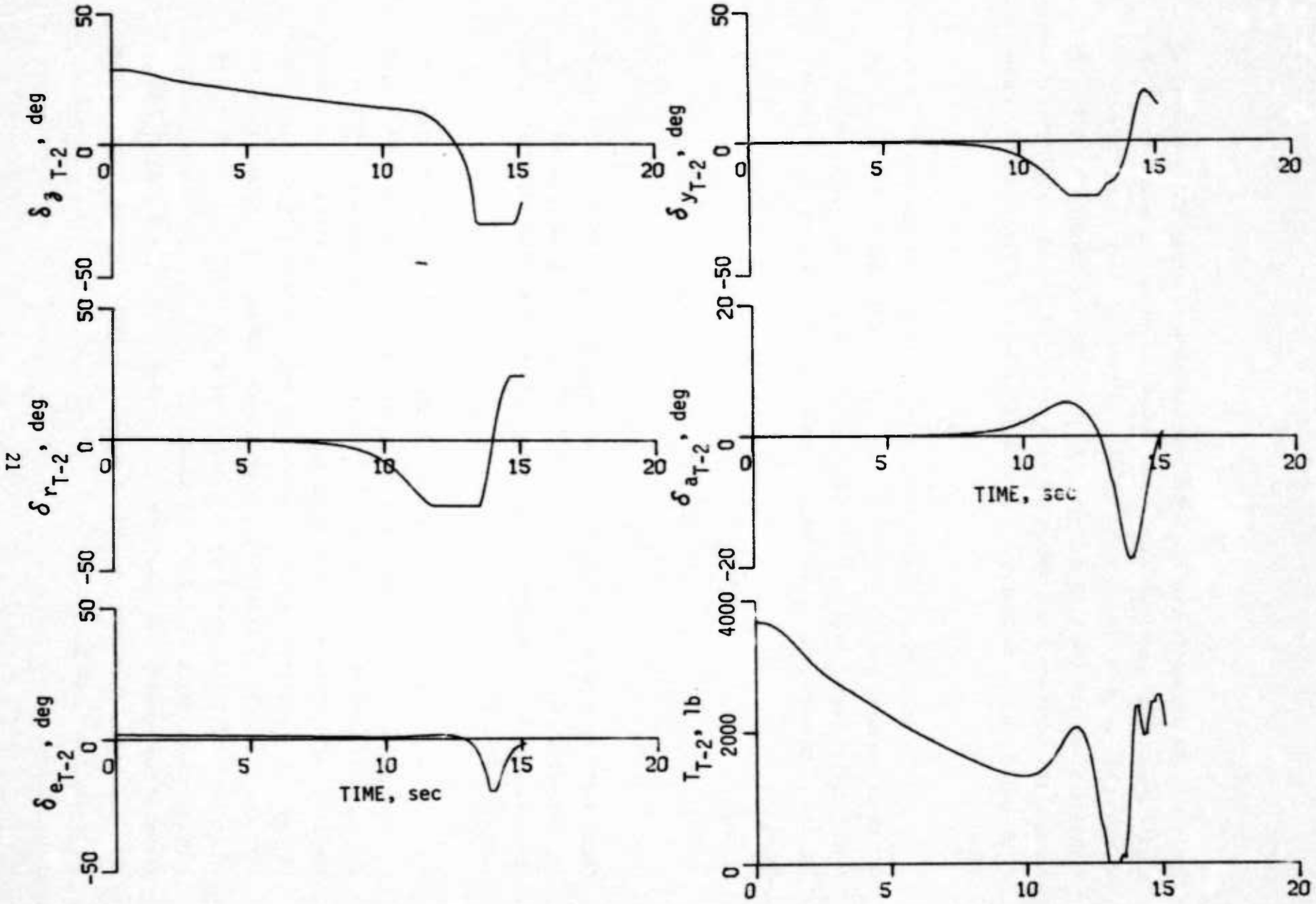

Figure 3.2 (concl'd) T-2 SIMULATION OF AN F-4 DEPARTURE, CLEAN CONFIGURATION

The inputs to the F-4 model are the same δ_e ramp and switching δ_a signal used in the previous case. The dynamic range of the model is 20° in α and $\pm 20^\circ$ in β . The quality of model following is excellent for the first 11.8 sec of the time history. At this time the rudder of the T-2 reaches its negative limit resulting in a deterioration in the quality of the r, β and n_y model following. The side force surfaces limit shortly thereafter.

The feedforward equations were solved by hand to ascertain the reason for these surfaces reaching their limits. It was determined that the large rudder deflection is necessary to match the sideslip of the model, which is -14.734°. In fact, the yawing moment feedforward equation at this time reduces to

$$\delta_{r_{T-2}} = \frac{-C_{n_{\beta_{T-2}}}}{C_{n_{\delta_{r_{T-2}}}}} \beta_m = 1.659 \beta_m \qquad (3.1)$$

Thus, 1.66° of rudder are needed to match every degree of β_m. Since the rudder deflection of the T-2 is limited to $\pm 25^\circ$, it will be able to match β_m excursions of $\pm 15^\circ$ maximum. This limitation is independent of flight condition and model aircraft.

A similar investigation was undertaken to determine the reason for the side-force surfaces limiting a short while after the rudder. Once again the generation of β_m has a large part to do with these surfaces limiting. The side-force surface effectiveness of the T-2 has been written in terms of $(\delta_y - \beta)$, the relative "angle of attack" of this surface. If the side-force surfaces had infinite effectiveness they would deflect β_m degrees since no additional deflection would be required to produce side force. With finite effectiveness they must deflect an amount beyond β_m to generate and match the side force which the model aircraft is producing. The sum of β_m plus this additional increment accounts for the side-force surfaces limiting when following the clean F-4 model.

Longitudinal control limits are encountered at 13.6 sec. into the time history when the thrust of the T-2 goes to zero and the direct-lift controls encounter their upper limit. The thrust goes to zero since α_m increases rapidly, increasing the drag of the F-4 and slowing it down. Analysis, similar to that for δ_r and δ_y, was performed to determine the reason for the direct-lift controls limiting. The linearized feedforward equations were solved to find the dominant terms contained in them which determine the direct lift surface deflections. The vast majority of lift generated by the direct lift control surfaces is required to match the angle of attack of the model. In fact, the lift feedforward equation can be approximated by

$$\delta_z \cong \frac{-C_{L\alpha_{T-2}}}{C_{L\delta_{z_{T-2}}}} \alpha_m \cong -4.03\,\alpha_m \qquad (3.2)$$

Therefore about 4° of δ_z are required to generate one degree of angle of attack. Since the travel of the direct-lift control surfaces is limited to $\pm 30^\circ$ a dynamic angle-of-attack range of 15° can be simulated, essentially independent of flight condition.

Reference 2.8 indicates that typical direct-lift flaps are rate limited at 40°/sec and the side-force surfaces are rate limited at 60°/sec. Applying these numbers to the example of this section indicates that the direct-lift flaps of the T-2 reach their rate limit just prior to the time they reach their position limit. The constraint imposed by the rate limit would not compromise the validity of the simulation to any great additional extent. The side-force surfaces of the T-2 did not reach their rate limit during this example.

A crude comparison was made between the departure parameters obtained from this simulation and flight test data. At best, fair agreement was obtained. For example, time histories presented in Reference 3.1 show that an F-4 during a nose slice achieved a maximum p of 75°/sec, a maximum r of 50°/sec and β excursions of $\pm 10^\circ$. The F-4 model developed for this study achieved a p of 125°/sec, r of 60°/sec and β of $\pm 18^\circ$ during a nose slice. Thus, the

results of this phase of the study should be tempered by the fact that the F-4 model used is more demanding than the actual aircraft.

With the exception of the n_z response, the T-2 simulated the F-4 behavior very well up to the departure point of the F-4, characterized by the nose slice behavior of the F-4. After the departure and into the incipient spin portion of the maneuver, the simulation is less accurate because of the control power limitations of the T-2. However, even after the departure, the angular motions of the airplane retain the same characteristics, as shown by the time histories of p, q, and r of Figure 3.2 and are probably more faithfully reproduced than is necessary for successful pilot training transfer.

3.3 Model-Following Results, A-7 Model

For Figure 3.3 the lateral-directional parameters of the model are characteristic of the A-7 while the longitudinal parameters of the F-4 are retained. The trim conditions are the same as in the previous case but the angle-of-attack mismatch is changed to 22°. The δ_e ramp and δ_a switching inputs are used again. Extremely large sideslips and $\Delta\alpha$'s are generated, 40° and 48° respectively, which are beyond the simulation capability of the T-2 as determined in the previous section. In fact, the quality of model following deteriorates after 6.6 sec when β exceeds 15° driving the T-2's rudder and side-force surfaces into saturation. The longitudinal controls are not limited until much later in the time history; in spite of this, the saturation of the δ_r and δ_y surfaces adversely affects the longitudinal model following because of coupling effects inherent in the T-2 equations of motion and aerodynamics. The time history is ended at 13.0 sec because the A-7 states are of a large magnitude and exceed the range of validity of the T-2 and feedforward equations. This resulted in wild fluctuations of the T-2's thrust.

3.1 McElroy, C., and Sharp, P., "Stall/Near Stall Investigation of the F-4E Aircraft", Air Force Flight Test Center, FTC-SD-70-20, October 1970.

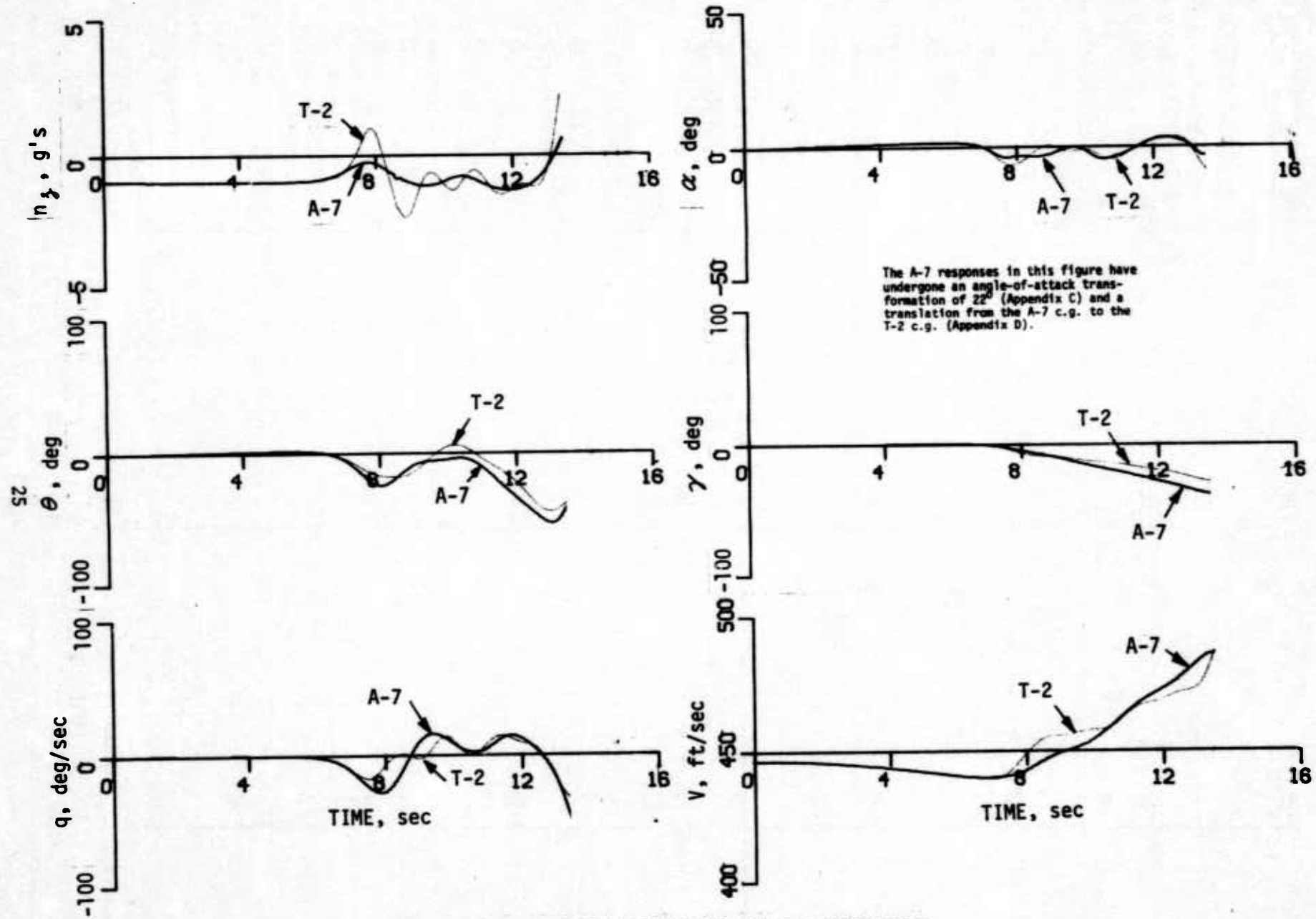

Figure 3.3 T-2 SIMULATION OF AN A-7 DEPARTURE

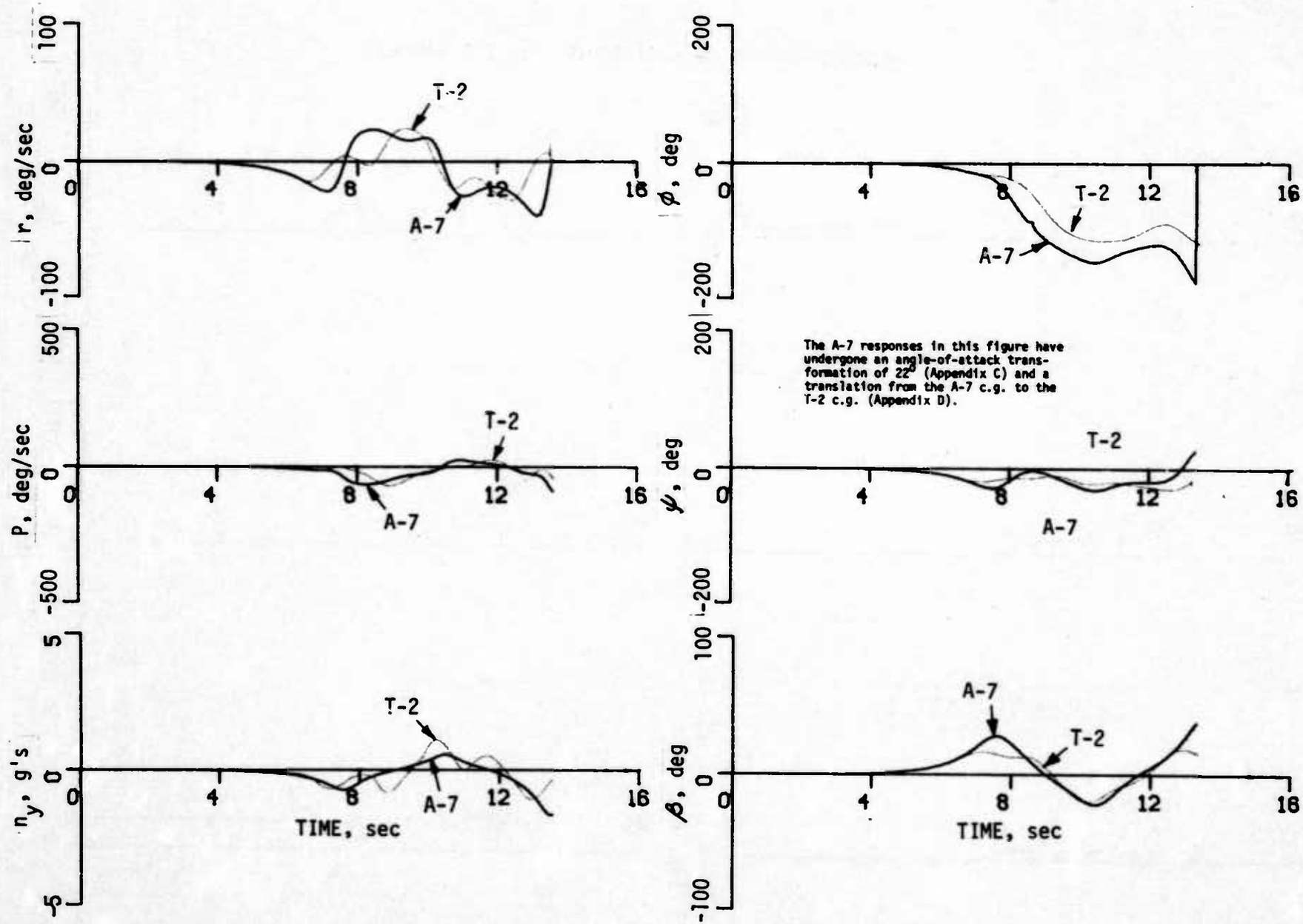

Figure 3.3 (cont'd) T-2 SIMULATION OF AN A-7 DEPARTURE

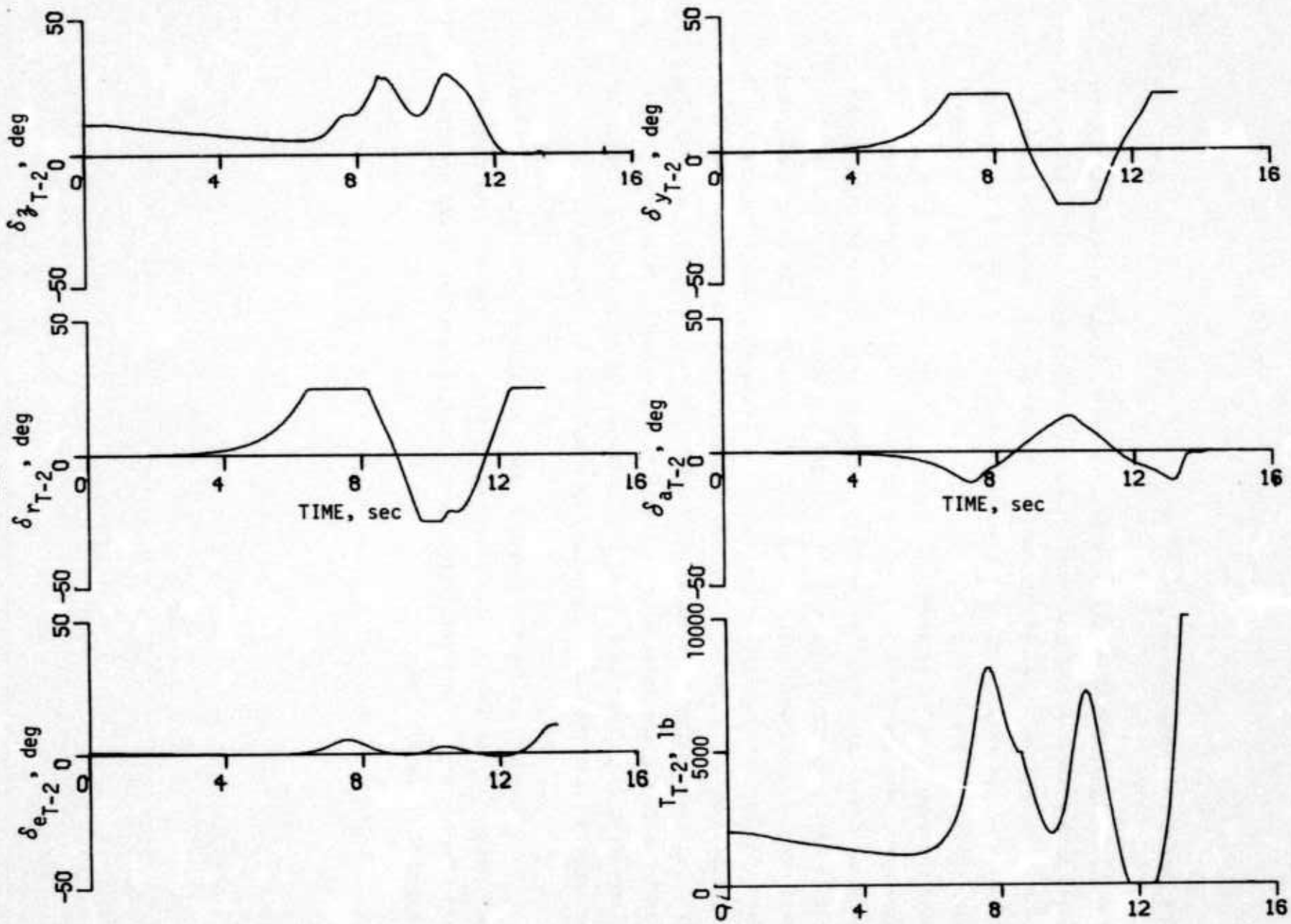

Figure 3.3 (concl'd) T-2 SIMULATION OF AN A-7 DEPARTURE

3.4 Model-Following Results, F-14 Model

Figure 3.4 shows the results of a T-2 following a departing model which incorporates F-14 aerodynamic characteristics. The model is trimmed at α_t = 26.586°, V_t = 446.68 fps and h = 10,000 ft. A departure did not result when the ramp δ_e and switching δ_a inputs, used in the previous examples, were applied to the F-14 model. -10° steps in δ_a and δ_r were used along with the ramp in δ_e to achieve one. Although a highly oscillatory spin developed, just the first five seconds of the time history are shown when the model is departing. For this particular example the quality of model following is excellent through departure until the $\Delta\alpha$ envelope range defined in this study is exceeded and the direct-lift flaps saturate at their upper limit. When this happens the longitudinal model following of course deteriorates, in particular n_z. As the F-14 angle of attack continues to increase, the F-14 lift begins to decrease, bending the flight path (γ) downward. The T-2 wing continues to provide increasing lift with the increase in θ and the T-2's direct lift flaps have to counter this to match the decreased F-14 lift. It is expected that the simulation would be terminated at this point.

However, unlike the previous case, coupling effects are not evident and the quality of lateral-directional model following remains good throughout the time history. The lateral-directional control surfaces do not saturate during the time history.

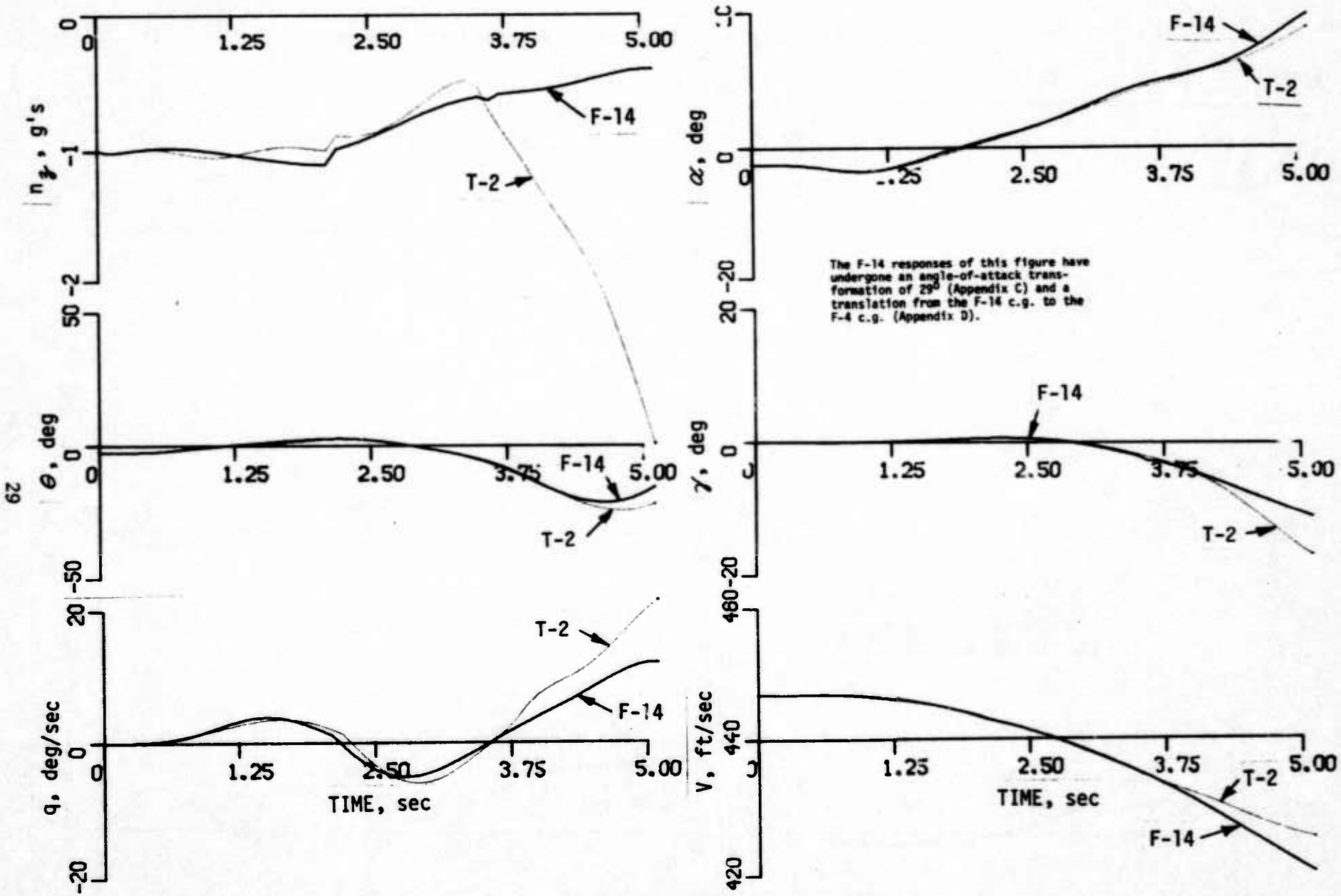

Figure 3.4 T-2 SIMULATION OF AN F-14 DEPARTURE

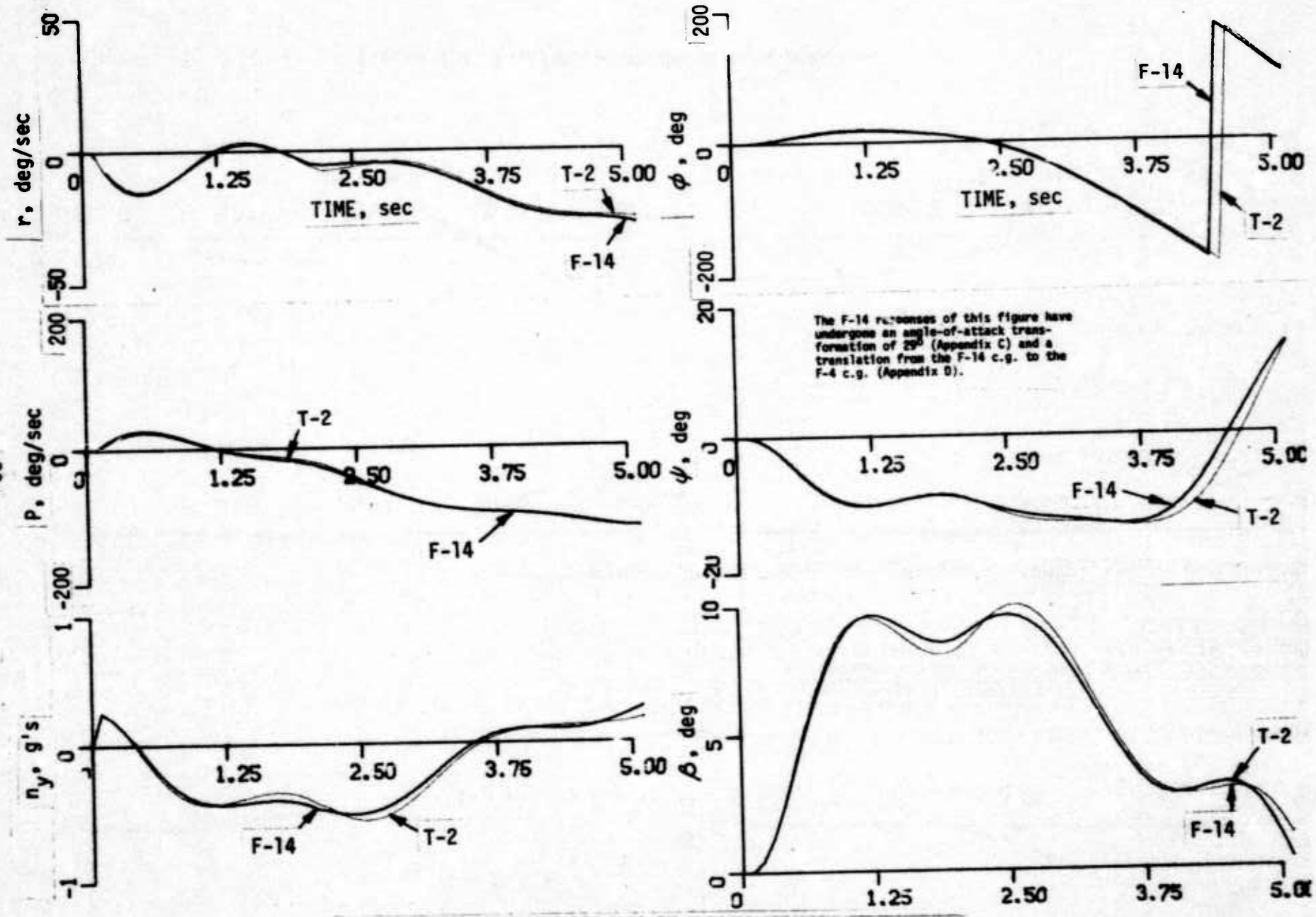

Figure 3.4 (cont'd) T-2 SIMULATION OF AN F-14 DEPARTURE.

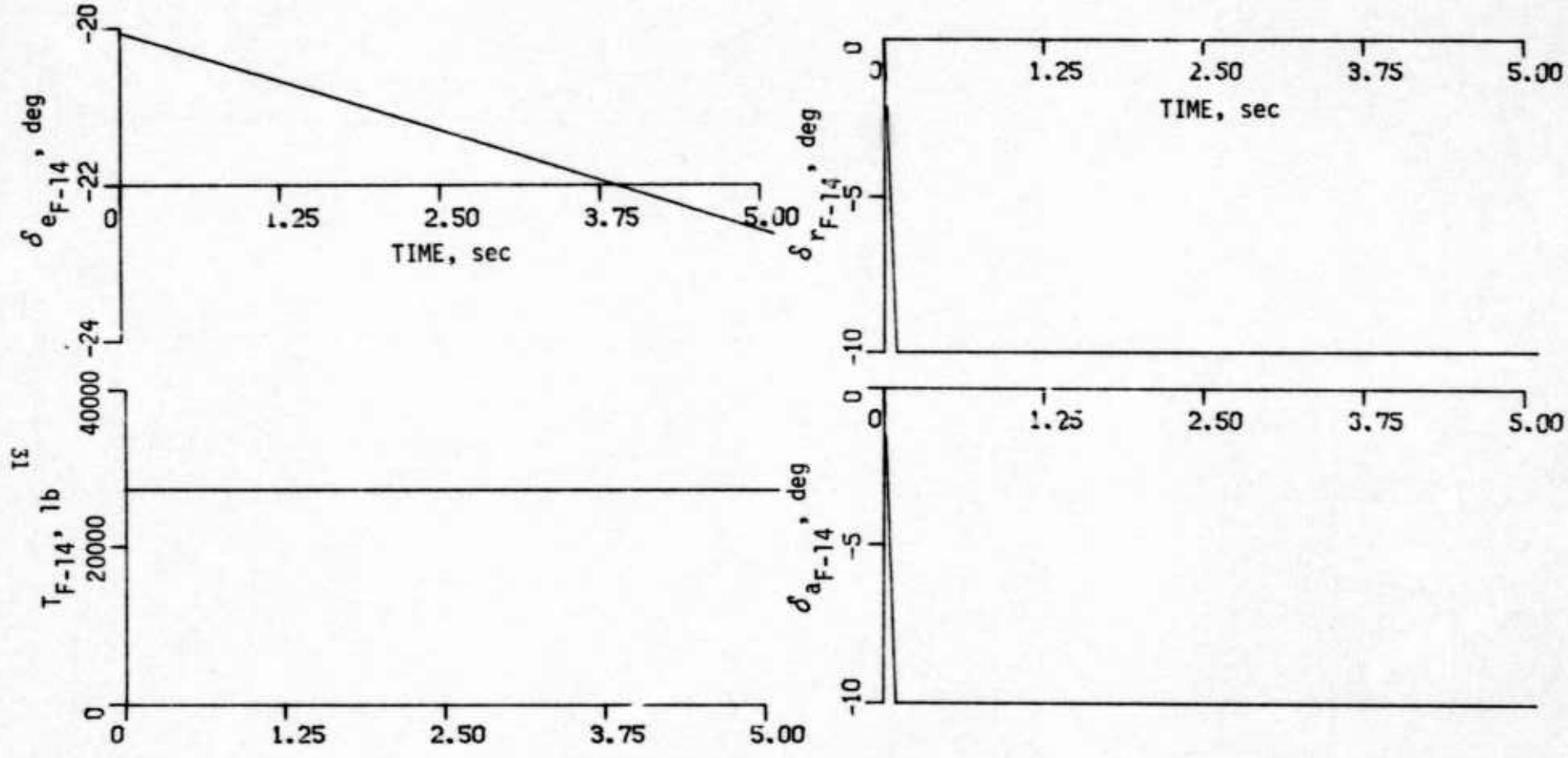

Figure 3.4 (cont'd) T-2 SIMULATION OF AN F-14 DEPARTURE

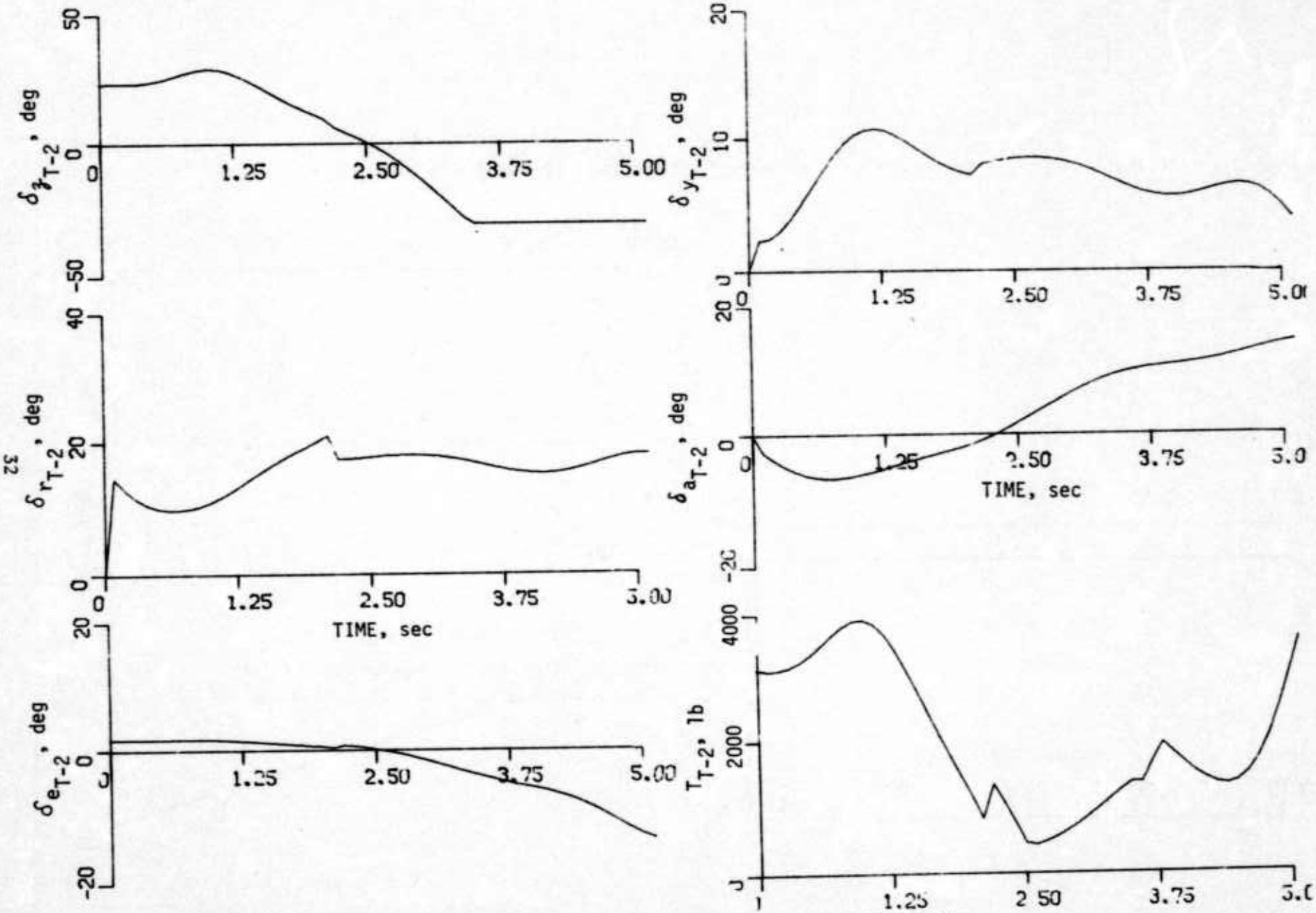

Figure 3.4 (concl'd) T-2 SIMULATION OF AN F-14 DEPARTURE

Section IV

ANGLE-OF-ATTACK AND SIDESLIP TRANSFORMATIONS

The results of the previous section indicate that the dynamic simulation envelope of the variable stability T-2 is limited to 15^{o} in angle of attack and $\pm 15^{o}$ in sideslip. It is also indicated that the model perturbations in angle of attack and sideslip may be up to three times as large. Therefore, methods of scaling, filtering, etc. the models' angle of attack and sideslip were investigated to determine if these variables could be reduced within the simulation envelope of the T-2.

Three transformations were investigated during the course of this study. The first is a constant scaling of sideslip and incremental angle of attack. The second involves the introduction of a velocity mismatch between the model aircraft and T-2 to effect a reduction in the angle-of-attack and sideslip signals of the model. Washout filters on these signals were also investigated. These filters reduce the low frequency content of the signals and may prevent the control surfaces from limiting as quickly. Results indicative of the effect of each of these techniques are presented and discussed.

4.1 Scaling of Sideslip and Incremental Angle of Attack

The first transformation discussed is a constant scaling of the sideslip and incremental angle-of-attack signals of the model. For this study the model aircraft was trimmed at 0^{o} sideslip. β_m was then modified by

$$\beta_T = K_\beta \beta_m \tag{4.1}$$

$$\dot{\beta}_T = K_\beta \dot{\beta}_m \tag{4.2}$$

where K_β is a scaling constant less than one to reduce the sideslip signal within the simulation envelope of the T-2. Similarly the angle-of-attack signal is modified according to

$$\alpha_T = \alpha_{t_m} + K_\alpha \Delta\alpha_m \tag{4.3}$$

$$\Delta\alpha_m = \alpha_m - \alpha_{t_m} \tag{4.4}$$

$$\dot{\alpha}_T = K_\alpha \dot{\alpha}_m \tag{4.5}$$

K_α is a scaling constant on $\Delta\alpha_m$ and less than one. The trim angle of attack was not affected by this transformation since it is dealt with using the technique of Section 2.4.

This technique was also chosen because of the fact that the pilot is not sensitive to angle of attack and sideslip in up-and-away flight and he would not be aware of the fact that the T-2 is matching the scaled values of $\Delta\alpha_m$ and β_m. It is desired to match the Euler angle rates of the model aircraft since these are felt to be important to a realistic simulation of the departing model aircraft. If the Euler angle rates and scaled $\Delta\alpha_m$ and β_m are matched by the T-2 the resultant linear accelerations of the T-2 are different from those of the model aircraft. The ramifications of this result should be investigated further since it is felt that a simulation of this nature may be quite suitable for the purposes under consideration in this study.

Modifying $\Delta\alpha_m$ and β_m implies that other variables must be changed to provide a consistent set governed by an airplanes equations of motion. These variables are u, v, w, $\dot{u}$, $\dot{v}$, $\dot{w}$, $\dot{h}$, h, γ, ρ, $\bar{q}$, Mn, n_x, n_y and n_z. They are computed from standard equations not presented here. The T-2 model follows the modified variables which are used in the control law to compute the control surface deflections of the T-2 required to achieve them. The rotational velocities and accelerations, the Euler angles and rates and the total velocity are not modified but used directly for model following.

The results obtained with this technique are presented in Figure 4.1 for the F-4 model in the clean configuration. The flight condition, inputs,

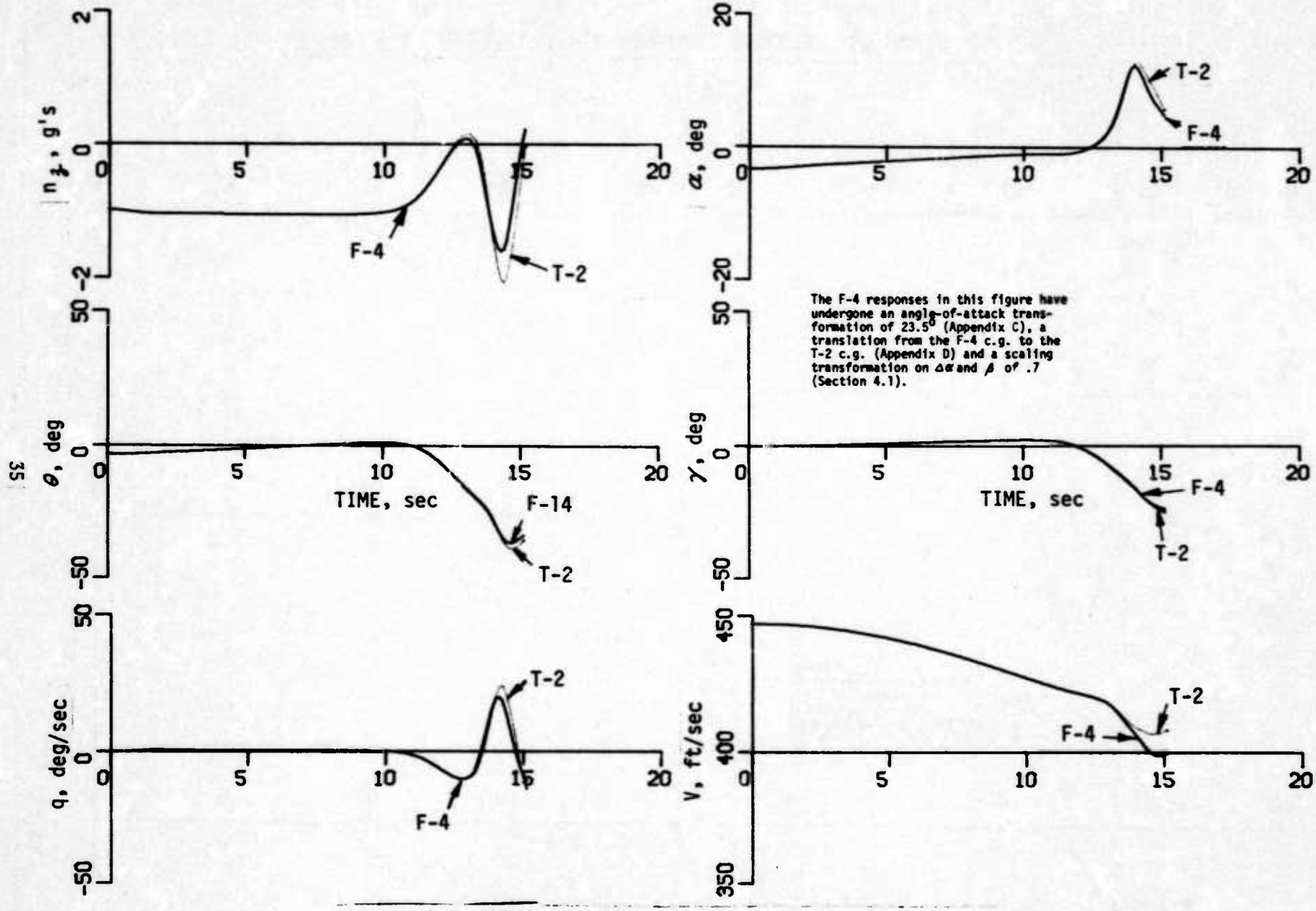

Figure 4.1 MODEL-FOLLOWING RESULTS, SCALING OF $\Delta\alpha_m$, β_m

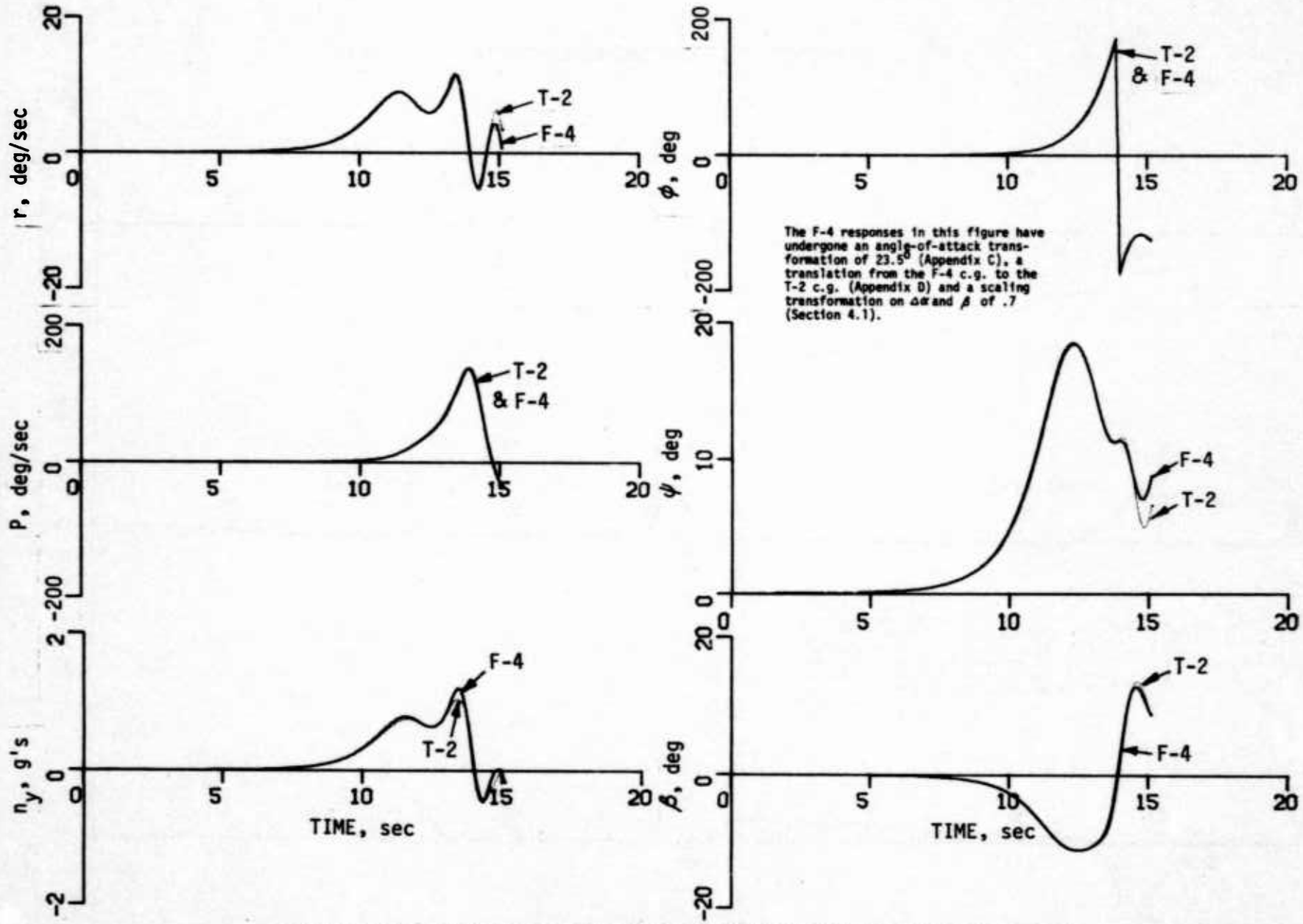

Figure 4.1 (cont'd) MODEL-FOLLOWING RESULTS, SCALING OF $\Delta\alpha_m$, β_m

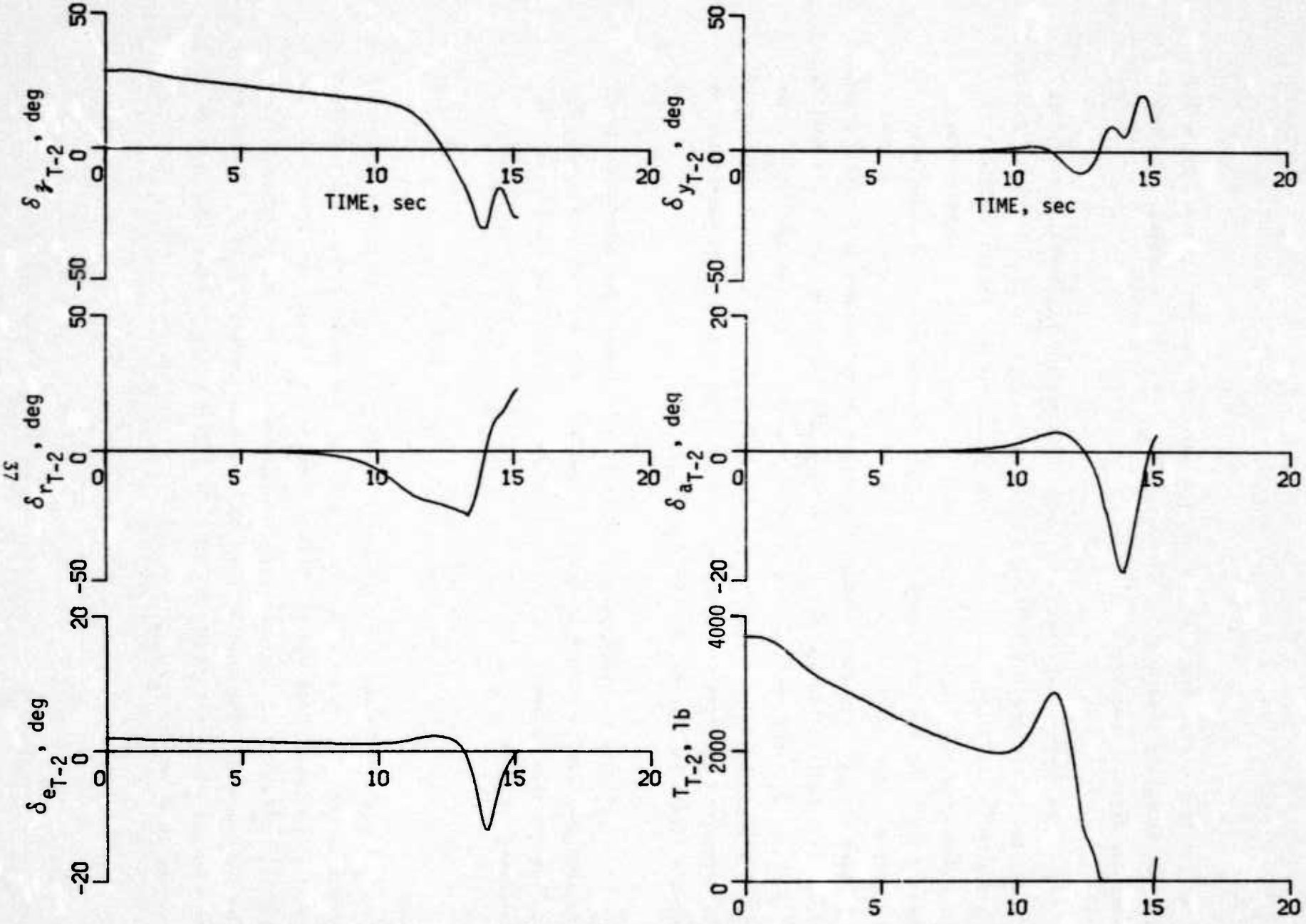

Figure 4.1 (concl'd) MODEL-FOLLOWING RESULTS, SCALING OF $\Delta\alpha_m$, β_m

trim conditions, etc. are the same as considered in Section 3.2 and Figure 3.2 with the exception that scaling factors of $K_\alpha = K_\beta = .7$ are used. The two cases are directly comparable.

The first thing that is evident in comparing Figures 4.1 and 3.2 is a reduction in the angle-of-attack and sideslip responses used for model following due to the scaling. This causes a change in the T-2 control deflections. The rudder does not limit at all and the side-force surfaces saturate only momentarily. The latter is also true for the direct-lift control surfaces. One very noticeable result of all of this is the very high quality of model following for all variables through the entire departure and 360° roll. Another effect is a modification of the n_{y_m} and n_{z_m} time histories due to the scaling of $\Delta\alpha_m$ and β_m. For example, the positive maximum of the modified n_{y_m} signal is 1.2 g's as opposed to a positive maximum of $\approx .5$ g's for the actual signal. The corresponding negative maxima are -.45 g's and -.83 g's, respectively. A similar effect is evident for the n_z signal.

Analysis was performed to determine the reason for the change in the acceleration signals resulting from the scaling. The n_y signal and the β_m scaling was given primary emphasis. It is best explained by considering the following equation

$$n_y = \frac{\dot{v} + ru - pw}{g} - \sin\phi\cos\theta \qquad (4.6)$$

r, p, ϕ and θ are not modified by the scaling of β_m. u and w are but the effect is minor because it is a $\cos\beta$ effect. The major change is a reduction in $\dot{v}$. Consider where the positive maximum of n_y occurs on Figure 4.1. The quantity $\dot{v} - pw$ is of the same order of magnitude as ru and of opposite sign. The two cancel leaving a relatively small term. The scaling of β reduces $\dot{v}$. $\dot{v} - pw$ and ru do not cancel to the same degree as in the previous case resulting in a larger n_y.

4.2 Velocity Mismatch Transformation

This technique involves the introduction of a velocity mismatch between the model aircraft and the T-2. That is, the velocity of the model was transformed by

$$V_T = V_m + K_V \tag{4.7}$$

$$\dot{V}_T = \dot{V}_m \tag{4.8}$$

where K_V is a positive constant increment of velocity. α_m and β_m are reduced since

$$\beta_T = \sin^{-1}\left(\frac{v_m}{V_T}\right) \tag{4.9}$$

$$\alpha_T = \sin^{-1}\left(\frac{w_m}{V_T \cos\beta_T}\right) \tag{4.10}$$

The variables u, $\dot{u}$, γ, h, $\dot{h}$, $\bar{q}$, ρ, M_n, n_x, n_y, n_z, $\dot{\alpha}$ and $\dot{\beta}$ must be recalculated to provide a consistent set. v_m and w_m are left unmodified along with the rotational and angular variables. The T-2's trim angle of attack must be modified to account for the increase in velocity. Instead of being trimmed at $\alpha_{t_{T-2}} = \alpha_{t_m} - i_m$ it must be trimmed at

$$\alpha_{t_T} = \sin^{-1}\left(\frac{V_{t_m} \sin\alpha_{t_{T-2}}}{V_T}\right) \tag{4.11}$$

assuming $\beta_T = 0$.

Results obtained employing the velocity mismatch transformation are given in Figure 4.2 for the case where the velocity of the T-2 is 100 fps. greater than that of the model aircraft. A comparison can be made between the results shown in this figure and Figures 3.2 and 4.1. In general, the results are quite similar to those presented in the previous section. The velocity mismatch has a less significant effect on δ_z than the scaling of $\Delta\alpha_m$ and β_m. Consequently, the longitudinal model following is poorer than in the previous

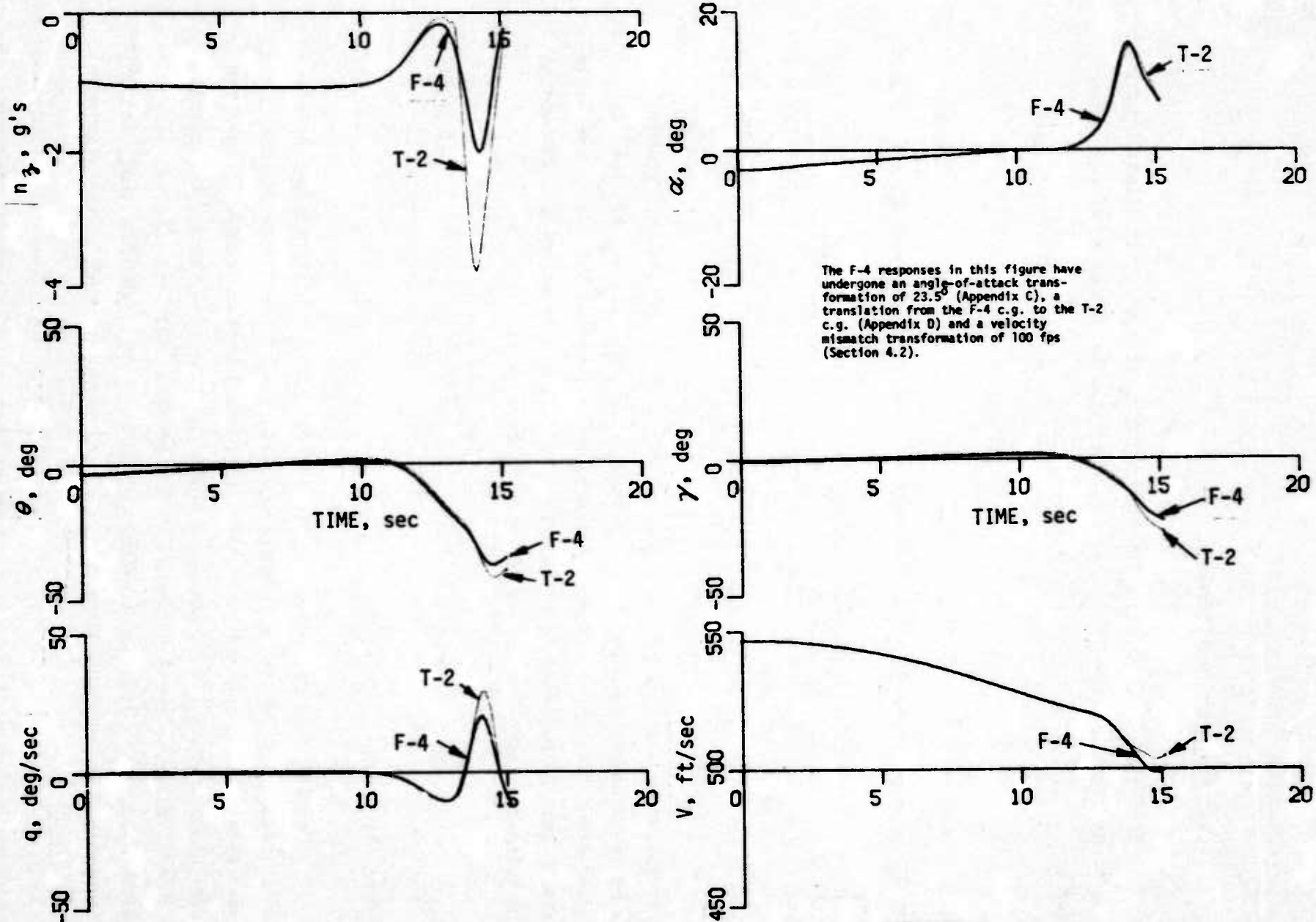

Figure 4.2 MODEL-FOLLOWING RESULTS, VELOCITY MISMATCH

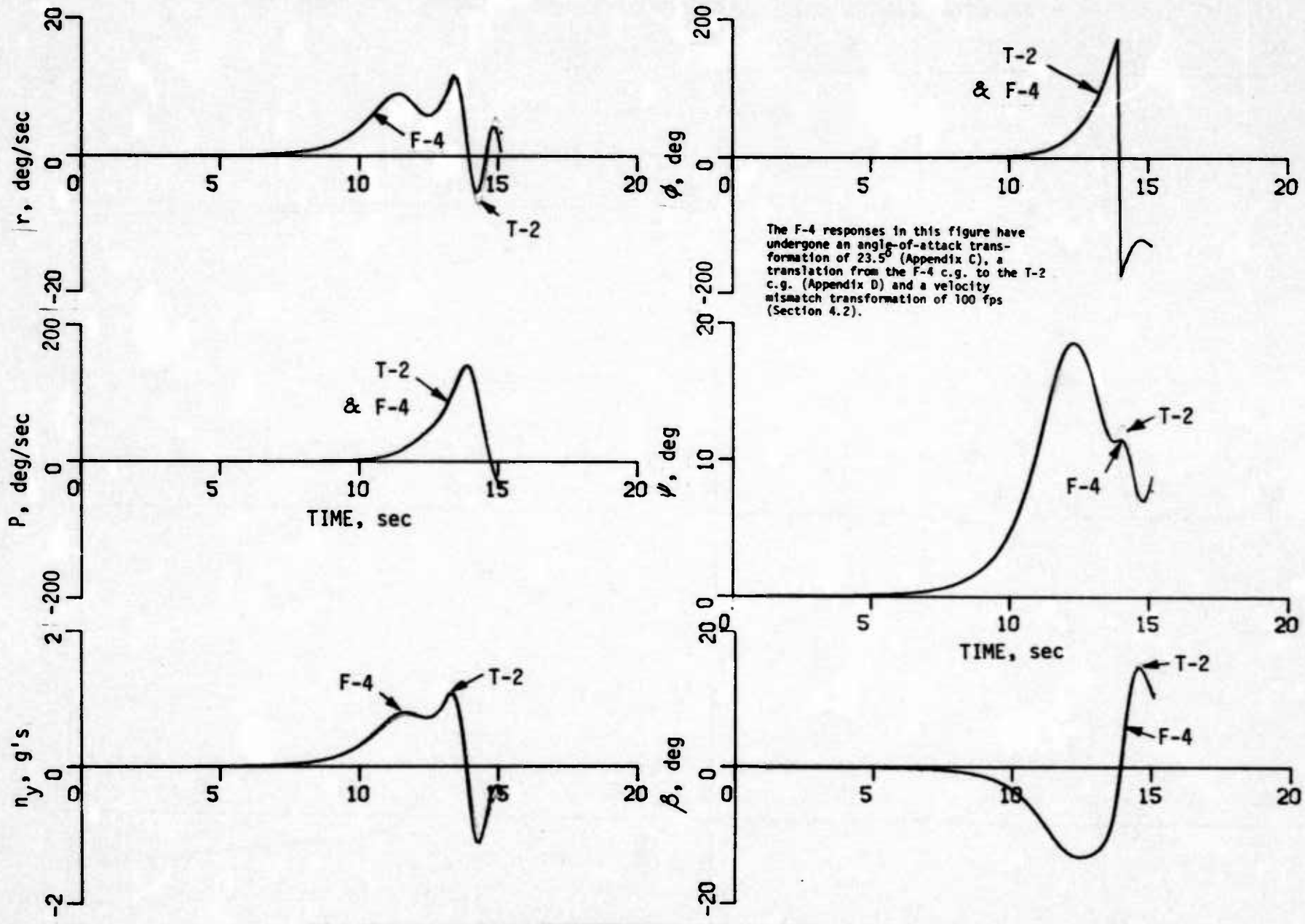

Figure 4.2 (cont'd) MODEL-FOLLOWING RESULTS, VELOCITY MISMATCH

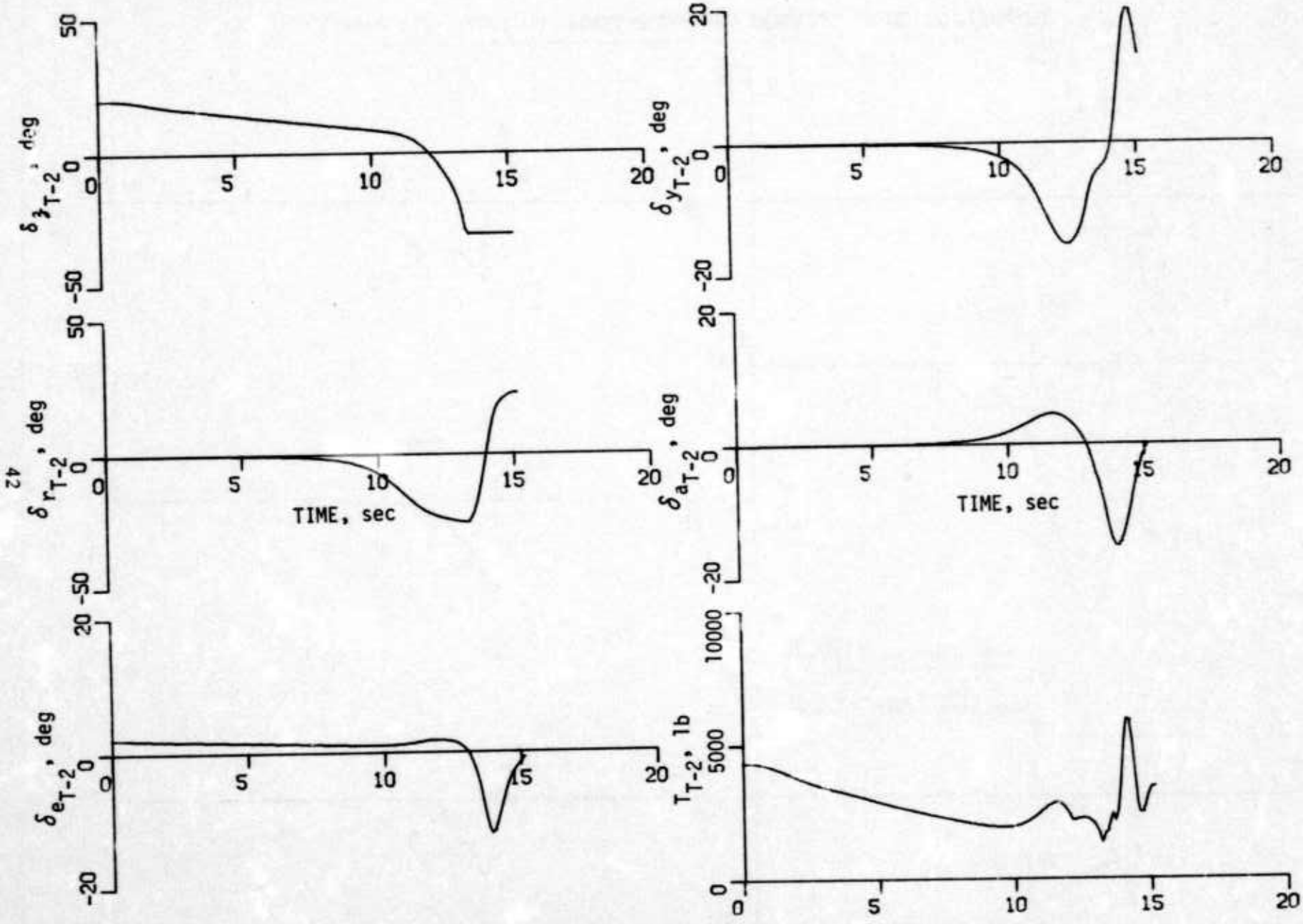

Figure 4.2 (concl'd) MODEL-FOLLOWING RESULTS, VELOCITY MISMATCH

case. This transformation also effects the n_y and n_z time histories. A consideration of Equation (4.6) leads to the conclusion that n_y is modified since the quantity u is changed and the change in u is a direct result of the velocity mismatch. Overall, this technique appears to be less suitable than the scaling of the sideslip and incremental angle of attack.

4.3 Washout Filtering of Sideslip and Angle of Attack

The last sideslip and angle-of-attack transformation investigated during this study involved the washout filtering of the signals to remove their low frequency content. The basic idea was that this approach would prolong the time before the control surfaces saturated. The angle-of-attack signal is transformed by

$$\alpha_T = \frac{\tau_\alpha s}{\tau_\alpha s + 1} \alpha_m \tag{4.12}$$

$$\dot{\alpha}_T = \frac{-\alpha_T}{\tau_\alpha} + \dot{\alpha}_m \tag{4.13}$$

and the β_m signal by

$$\beta_T = \frac{\tau_\beta s}{\tau_\beta s + 1} \beta_m \tag{4.14}$$

$$\dot{\beta}_T = \frac{-\beta_T}{\tau_\beta} + \dot{\beta}_m \tag{4.15}$$

where τ_α and τ_β are the time constants of the filters. The additional variables which must be recomputed because of this transformation are the same as for the scaling of sideslip and incremental angle of attack.

The results obtained employing just the β washout filter are presented in Figure 4.3 for $\tau_\beta = 5$. The same case considered for the other two transformations is used to provide a direct comparison of results. As before, both the n_y and n_z signals are modified by the transformation. The use of washout filtering prevented the rudder of the T-2 from reaching saturation during its first negative swing which is unlike the nominal case (Figure 3.2). However,

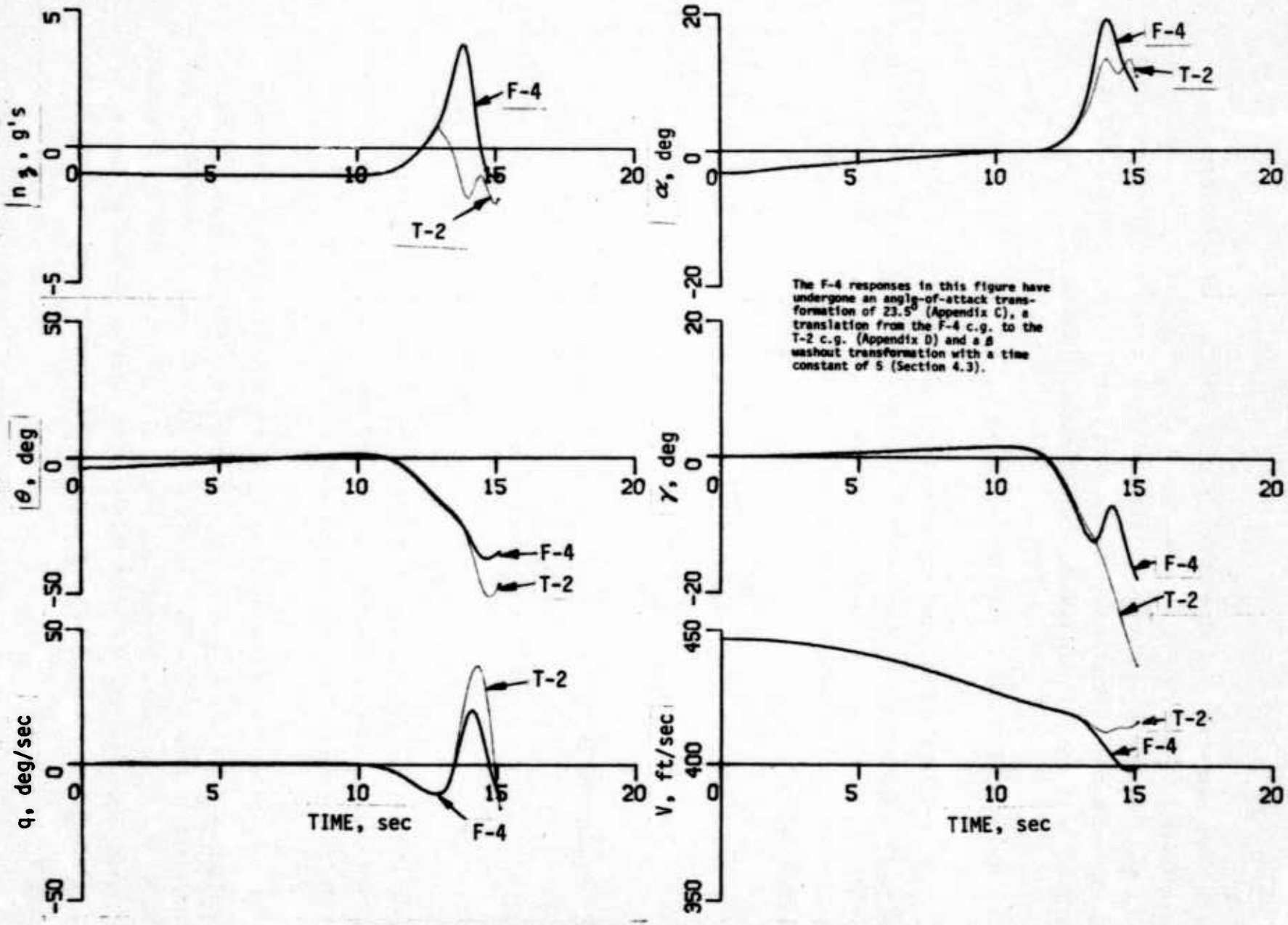

Figure 4.3 MODEL-FOLLOWING RESULTS, β_m WASHOUT

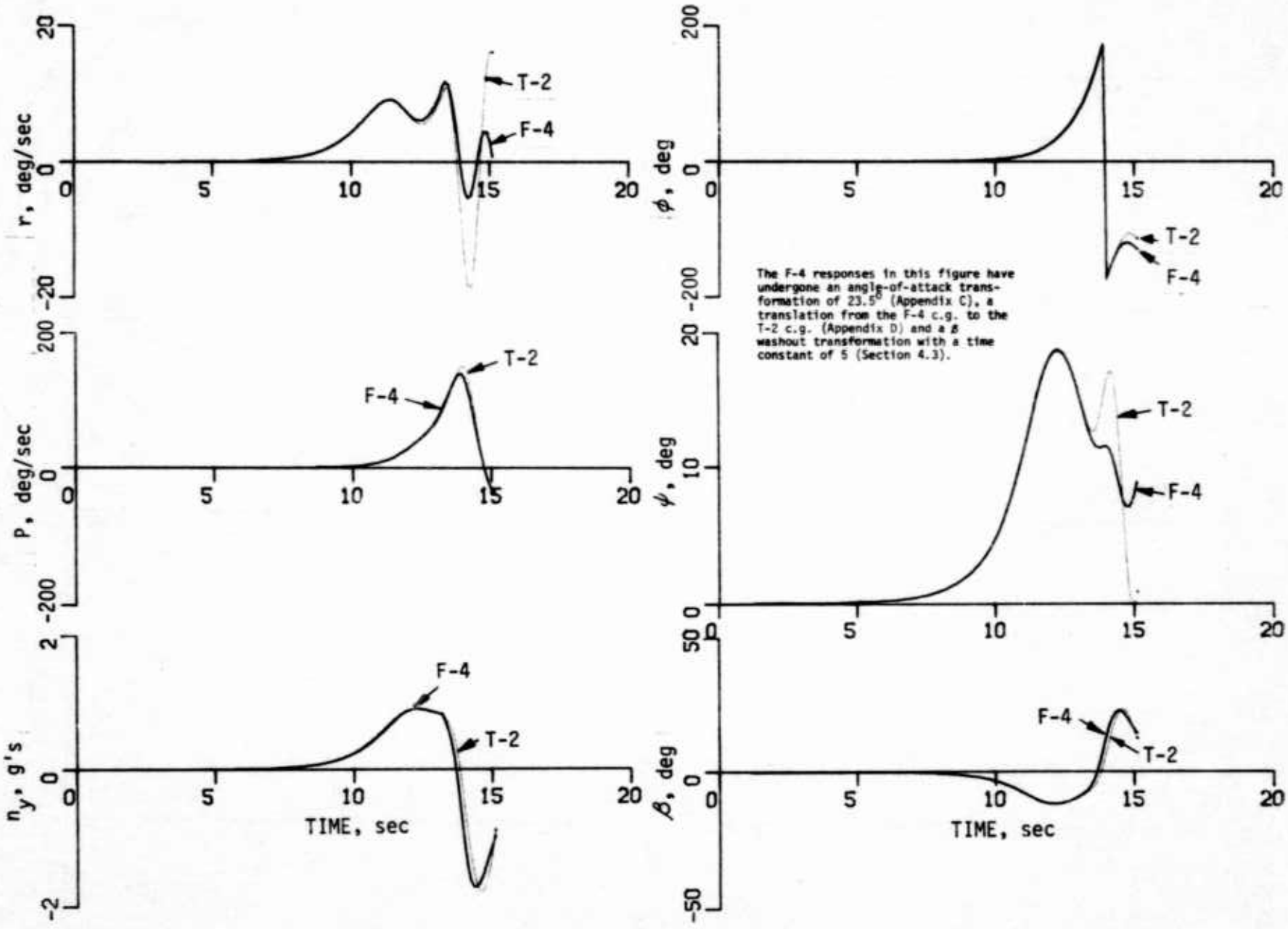

Figure 4.3 (cont'd) MODEL-FOLLOWING RESULTS, β_m WASHOUT

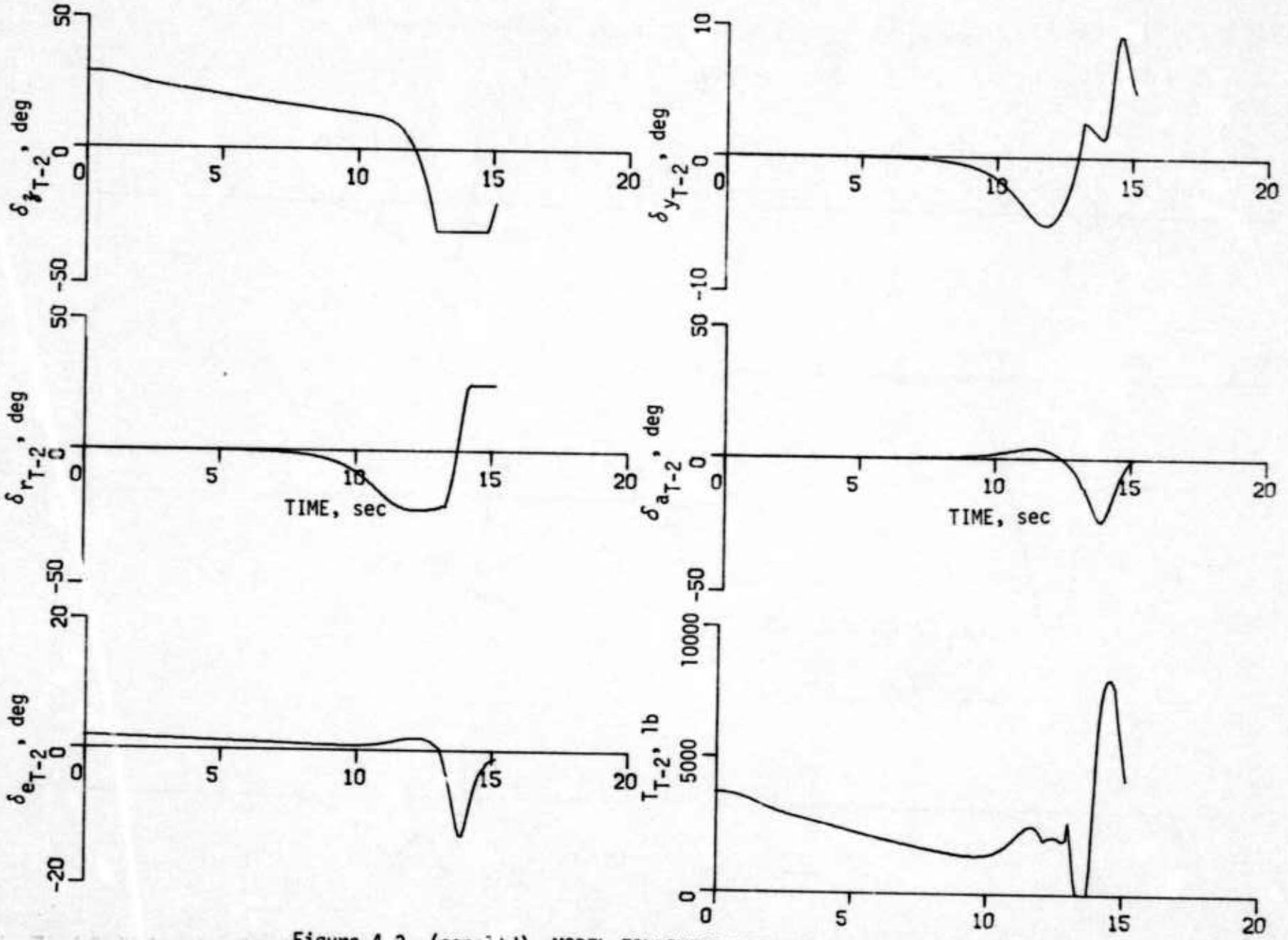

Figure 4.3 (concl'd) MODEL-FOLLOWING RESULTS, β_m WASHOUT

it saturated when it deflected positive as in the nominal case. The side-force surfaces did not saturate as they did in Figure 3.2. The consequences of these facts is that the washout filtering of the models sideslip resulted in improved lateral-directional model following. The quality of the longitudinal model following was essentially unaltered since a washout filter on angle of attack was not used.

Section V

SUMMARY, CONCLUSIONS AND RECOMMENDATIONS

The intent of this study was to determine the high angle-of-attack simulation capability of a T-2 configured for variable stability operation. It was also desired to ascertain the envelope over which a variable stability T-2 can reproduce the motions of the model aircraft (which exhibited characteristics typical of various airplanes in the Navy inventory). A digital simulation of a variable stability T-2 model-following system was developed and employed for these purposes. The results of this study indicate that it is feasible to employ the T-2 as a variable stability high angle-of-attack simulator. Time histories included in the report show that a variable stability T-2 can faithfully reproduce all motions of the model aircraft prior to departure and after departure within an envelope defined by 15^{o} in incremental angle of attack and $\pm$ 15^{o} in sideslip as calculated from the stability and control derivatives of the T-2. In spite of this, a variable stability T-2 has definite merit as a high angle-of-attack simulator since it can be used to provide a means for investigating the fringe of the controllability flight regime. A variable stability T-2 can be used to explore near departure control problems and allow pilots to learn how close to the boundary they can fly in the incipient departure region of flight.

An additional goal of this study was to explore techniques for providing simulation capability beyond the 15^{o} in incremental angle of attack and $\pm$ 15^{o} in sideslip. It is desired to match the Euler angles and rates of the model aircraft since these are felt to be important to a realistic simulation of the departure modes. It was decided to modify the angle of attack and sideslip of the model aircraft since the pilot is not directly sensitive to these variables in up and away flight and he would not be aware of the fact that the T-2 is matching transformed variables. Three techniques for expanding the simulation envelope were explored and found to show promise. The most successful one involved the scaling down of $\Delta\alpha_m$ and β_m by a constant. However, as a consequence of employing the transformations, the linear accelerations which

the T-2 undergoes will be different from those of the model aircraft. The ramifications of this result should be investigated further since it is quite possible that a simulation of this nature may be suitable for the intended purpose.

Other conclusions have also been reached during the course of this study and are listed below.

1. A constant angle-of-attack transformation between the model and T-2 should be used to provide the widest useful simulation with the T-2. This allows the model to be trimmed at a high angle of attack near its departure boundary and the T-2 to be trimmed at a small or negative angle of attack.

2. The model-following system developed during this study can be implemented in an airborne digital computer. No unusual equipment is required for it.

3. The model-following control law developed for the T-2 high angle-of-attack simulator is straightforward and not overly complex. It assumes that the T-2 aerodynamic, mass and inertial characteristics are known exactly, so for practical use in an in-flight simulator, the feedback loops should be added (they were unnecessary in this study).

4. The aerodynamics of the model aircraft should be implemented in table look-up form to avoid errors in fitting the data, extremely high order polynomial fits, etc..

5. A combination of speed brake and throttle may be required for X-force control and reinforces a similar conclusion reached in an earlier study investigating the feasibility of employing the T-2 as an in-flight simulator. Other means of obtaining additional drag should be investigated.

There are seven major areas where it is recommended that additional study be initiated with regard to employing the T-2 as a high angle-of-attack simulator. They are:

1. Investigations should be conducted to develop aircraft models which can be used to simulate additional modes of high angle-of-attack behavior, e.g. "wing rock."

2. The use of the T-2 as a spin simulator should be investigated. The forces and moments required to make the T-2 spin like other aircraft can be computed. The feasibility of employing additional force and moment generating devices can be determined.

3. A study should be initiated to investigate feedback gain design for the T-2 high angle-of-attack simulator. The use of feedback lessens model-following errors and may permit simplifications in the control law.

4. Attention should be given to the implementation of the model-following system in a digital computer similar to one which may be used in flight. Items such as the effects of sampling time, computation delay, etc. should be considered.

5. Additional methods for transforming the angle of attack and sideslip of the model into the simulation envelope of the T-2 should be researched. Just a few techniques have been looked at in this study but many more possibilities exist.

6. No quantitative judgments or evaluations were made to determine the minimum acceptable model-following errors. Engineering judgment was used to weight incremental attitude matching more heavily than other variables. A better definition of the relative importance of each of the variables to the departure training situation would be very useful. It would be an error

to design a training simulator that either oversimulates or undersimulates.

7. Time histories from the high angle-of-attack flights of aircraft in the Navy inventory should be used as inputs to the variable stability T-2 model-following control law to obtain a better idea of how well the T-2 will be able to reproduce the motions of these aircraft in the departure flight regime.

APPENDIX A

SIX DEGREE-OF-FREEDOM MODEL AIRCRAFT EQUATIONS

The force equations are

$$[\dot{V}] = \begin{bmatrix} \dot{u} \\ \dot{v} \\ \dot{w} \end{bmatrix} = \frac{1}{m} \cdot [F] - [\omega_x] \cdot [V]$$

The moment equations are

$$[\dot{\omega}] = \begin{bmatrix} \dot{p} \\ \dot{q} \\ \dot{r} \end{bmatrix} = [I]^{-1} \cdot \left([M] - [\omega_x] \cdot \{ [I] \cdot [\omega] \} \right)$$

where $$[F] = [F_{AERO}] + [F_{THRUST}] + [F_{GRAV}]$$

$$[F_{AERO}] = \bar{q} \cdot S \cdot \begin{bmatrix} C_x \\ C_y \\ C_z \end{bmatrix}$$

$$[F_{GRAV}] = m \cdot g \cdot \begin{bmatrix} -\sin\theta \\ \sin\phi \cdot \cos\theta \\ \cos\phi \cdot \cos\theta \end{bmatrix}$$

$$[\omega_x] = \begin{bmatrix} 0 & -r & q \\ r & 0 & -p \\ -q & p & 0 \end{bmatrix}$$

$$[I] = \begin{bmatrix} I_{xx} & 0 & -I_{xz} \\ 0 & I_{yy} & 0 \\ -I_{xz} & 0 & I_{zz} \end{bmatrix}$$

$$[M] = [M_{AERO}] + [M_{THRUST}]$$

$$[M_{AERO}] = \bar{q} \cdot S \cdot \begin{bmatrix} b & 0 & 0 \\ 0 & \bar{c} & 0 \\ 0 & 0 & b \end{bmatrix} \cdot \begin{bmatrix} C_\ell \\ C_m - (C_z \cdot \Delta CG) \\ C_n + (C_y \cdot \Delta CG \frac{\bar{c}}{b}) \end{bmatrix}$$

The auxiliary equations for angle of attack and sideslip are:

$$\alpha = \sin^{-1}\left(\frac{w}{V \cos \beta}\right)$$

$$\beta = \sin^{-1}\left(\frac{v}{V}\right)$$

The Euler angles are obtained from the integration of the following equation:

$$\begin{bmatrix} \dot{\phi} \\ \dot{\theta} \\ \dot{\psi} \end{bmatrix} = \begin{bmatrix} 1 & \sin\phi \tan\theta & \cos\phi \tan\theta \\ 0 & \cos\phi & -\sin\phi \\ 0 & \sin\phi \sec\theta & \cos\phi \sec\theta \end{bmatrix} \begin{bmatrix} p \\ q \\ r \end{bmatrix}$$

APPENDIX B

T-2 AERODYNAMICS

$$C_{L_{U.T.}} = \left[0.846 - 0.307Mn + 0.823Mn^2\right]\left[1 - 0.255\left(\frac{\beta}{10}\right)^2\right]\left[\frac{\alpha}{10}\right]$$

$$C_L = C_{L_{U.T.}} + \left[0.086 - 0.0224\left(1 + 1.67e^{-\frac{h}{27180}}\right)Mn^2\right]\left[\frac{\delta_e}{10}\right]$$
$$+ \left[0.209\left(\frac{\delta_z}{10}\right) - 0.00315\left(\frac{\delta_z}{10}\right)^3\right]$$
$$+ \left[-0.045 + 0.0375\left(\frac{\alpha}{10}\right)\right]K_{L.G.} + \left[0.0525 + 0.241\left(\frac{\alpha}{10}\right)\right]T_c'$$

$$C_D = 0.02 + 0.0798\,C_{L_{U.T.}}^2$$
$$+ \left[0.0216\left|\frac{\delta_z}{10}\right| + 0.01583\left(\frac{\alpha}{10}\right)\left(\frac{\delta_z}{10}\right) + 0.00112\left(\frac{\delta_z}{10}\right)^2\right]$$
$$+ 0.01\left(\frac{\delta_y - \beta}{10}\right)^2 + \left[0.031 - 0.005\left(\frac{\alpha}{10}\right)^2\right]K_{L.G.} - T_c'$$

$$\begin{bmatrix} C_x \\ C_z \end{bmatrix} = \begin{bmatrix} -\cos\alpha & \sin\alpha \\ -\sin\alpha & -\cos\alpha \end{bmatrix}\begin{bmatrix} C_D \\ C_L \end{bmatrix}$$

$$C_y = \left[-0.149\left(\frac{\beta}{10}\right) - 0.00267\left(\frac{\beta}{10}\right)^3\right] + 0.0183\left(\frac{\delta_r}{10}\right)$$
$$+ \left[-0.0283 + 0.03054\left(\frac{\alpha}{10}\right)\right]\frac{p}{V}$$
$$+ 0.150\left(\frac{\delta_y - \beta}{10}\right) - 0.0112\left(\frac{\delta_y - \beta}{10}\right)^3$$

$$C_{m_{0.25\bar{c}}} = \left[0.0368 - 0.0364\,Mn + 0.0518\,Mn^2\right]$$

$$+ \left[-0.148 + 0.0918\left(1 + 0.756\,e^{-\frac{h}{28742}}\right)Mn^2\right]\left[1 - 0.03\left(\frac{\beta}{10}\right)^2\right]\left[\frac{\alpha}{10}\right]$$

$$+ \left[1 - 0.233\left(1 + 1.76\,e^{-\frac{h}{28000}}\right)Mn^2\right]\left[-0.276\left(\frac{\delta_e}{10}\right) + 0.0226\left(\frac{\delta_e}{10}\right)^3\right]$$

$$+ \left[-0.693 + 0.131\,Mn - 0.407\,Mn^2\right]\left[\frac{q}{V}\right]$$

$$+ \left[-0.236 - 0.2947\,Mn^2\right]\left[\frac{\alpha}{V}\right]$$

$$+ \left[0.21 + 0.104\left(\frac{\alpha}{10}\right)\right]T_c'$$

$$+ \left[-0.004 + 0.142\left(\frac{\alpha}{10}\right)\right]\left(\frac{\delta_z}{10}\right) - 0.004\,K_{L.G.}$$

$$C_l = \left[-0.0247\left(\frac{\beta}{10}\right) + 0.000708\left(\frac{\beta}{10}\right)^3\right]\left[1 - 0.0607\left(\frac{\alpha}{10}\right)\right]$$

$$- 0.0319\left(\frac{\delta_a}{10}\right) + 0.00223\left(\frac{\delta_r}{10}\right) - 0.176\,\frac{p}{V}$$

$$+ \left[0.0333 + 0.03886\left(\frac{\alpha}{10}\right)\right]\left(\frac{r}{V}\right)$$

$$C_{n_{0.25\bar{c}}} = 0.0147\left(\frac{\beta}{10}\right) - 0.00886\left(\frac{\delta_r}{10}\right)$$

$$- 0.0167\left(\frac{\alpha}{10}\right)\frac{p}{V} - 0.0499\left(\frac{r}{V}\right)$$

APPENDIX C

ANGLE-OF-ATTACK TRANSFORMATION

The angle of attack of the model is transformed by

$$\alpha_T = \alpha_m - i_m$$

$$\dot{\alpha}_T = \dot{\alpha}_m$$

A transformation matrix is defined as

$$\mathcal{T} = \begin{bmatrix} \cos i_m & 0 & \sin i_m \\ 0 & 1 & 0 \\ -\sin i_m & 0 & \cos i_m \end{bmatrix}$$

Additional model variables are then transformed as follows

$$\begin{bmatrix} u \\ v \\ w \end{bmatrix}_T = \mathcal{T} \begin{bmatrix} u \\ v \\ w \end{bmatrix}_m \qquad \begin{bmatrix} \dot{u} \\ \dot{v} \\ \dot{w} \end{bmatrix}_T = \mathcal{T} \begin{bmatrix} \dot{u} \\ \dot{v} \\ \dot{w} \end{bmatrix}_m$$

$$\begin{bmatrix} p \\ q \\ r \end{bmatrix}_T = \mathcal{T} \begin{bmatrix} p \\ q \\ r \end{bmatrix}_m \qquad \begin{bmatrix} \dot{p} \\ \dot{q} \\ \dot{r} \end{bmatrix}_T = \mathcal{T} \begin{bmatrix} \dot{p} \\ \dot{q} \\ \dot{r} \end{bmatrix}_m$$

$$\begin{bmatrix} n_x \\ n_y \\ n_z \end{bmatrix}_T = \mathcal{T} \begin{bmatrix} n_x \\ n_y \\ n_z \end{bmatrix}_m \qquad \begin{bmatrix} \ell_x \\ \ell_y \\ \ell_z \end{bmatrix}_T = \mathcal{T} \begin{bmatrix} \ell_x \\ \ell_y \\ \ell_z \end{bmatrix}_m$$

The Euler angles are transformed according to

$$\theta_T = \sin^{-1}\left[\cos i_m \sin\theta_m - \sin i_m \cos\theta_m \cos\phi_m\right]$$

$$\phi_T = \sin^{-1}\left[\frac{1}{\cos\theta_T}\left(\sin\phi_m \cos\theta_m\right)\right]$$

$$\psi_T = \cos^{-1}\left[\frac{1}{\cos\theta_T}\left\{\begin{array}{l}\cos i_m \cos\theta_m \cos\psi_m \\ + \sin i_m\left(\sin\theta_m \cos\phi_m \cos\psi_m + \sin\phi_m \sin\psi_m\right)\end{array}\right\}\right]$$

The Euler angle rates are obtained from the following equations

$$\dot{\theta}_T = q_T \cos\phi_T - r_T \sin\phi_T$$

$$\dot{\phi}_T = p_T + \dot{\psi}_T \sin\theta_T$$

$$\dot{\psi}_T = \frac{1}{\cos\theta_T}\left[q_T \sin\phi_T + r_T \cos\phi_T\right]$$

The following variables are left invariant by the transformation

$$V_T = V_m \qquad \dot{V}_T = \dot{V}_m$$

$$\gamma_T = \gamma_m \qquad \dot{\gamma}_T = \dot{\gamma}_m$$

$$h_T = h_m \qquad \dot{h}_T = \dot{h}_m$$

$$\beta_T = \beta_m \qquad \dot{\beta}_T = \dot{\beta}_m$$

APPENDIX D
TRANSLATION EQUATIONS

A set of aircraft variables is defined at a point in space. A new set of variables is to be defined at a new point in space differing from the original one by ℓ_x feet along the x-body axis and ℓ_z feet along the z-body axis. The following equations define the variables affected by this transformation which are denoted by subscript T. Variables unaffected by this transformation are not listed.

$$u_T = u + q\ell_z \qquad \dot{u}_T = \dot{u} + \dot{q}\ell_z$$

$$v_T = v + r\ell_x - p\ell_z \qquad \dot{v}_T = \dot{v} + \dot{r}\ell_x - \dot{p}\ell_z$$

$$\omega_T = \omega - q\ell_x \qquad \dot{\omega}_T = \dot{\omega} - \dot{q}\ell_x$$

$$n_{x_T} = n_x + \frac{1}{g}\left[\dot{q}\ell_z + rp\ell_z - (r^2 + q^2)\ell_x\right]$$

$$n_{y_T} = n_y + \frac{1}{g}\left[\dot{r}\ell_x - \dot{p}\ell_z + pq\ell_x + rq\ell_z\right]$$

$$n_{z_T} = n_z + \frac{1}{g}\left[-\dot{q}\ell_x + pr\ell_x - (q^2 + p^2)\ell_z\right]$$

$$V_T = \sqrt{u_T^2 + v_T^2 + \omega_T^2}$$

$$\beta_T = \sin^{-1}(v_T / V_T)$$

$$\alpha_T = \sin^{-1}(\omega_T / V_T \cos\beta_T)$$

$$\dot{V}_T = \frac{(u_T\dot{u}_T + v_T\dot{v}_T + \omega_T\dot{\omega}_T)}{V_T}$$

$$\alpha_T = \frac{u_T\dot{\omega}_T - \dot{u}_T\omega_T}{u_T^2 + \omega_T^2}$$

$$\beta_T = \frac{\dot{v}_T - v_T V_T}{V_T\sqrt{V_T^2 - v_T}}$$

APPENDIX E

MODEL-FOLLOWING CONTROL LAW

It is desired to have the T-2 match the model responses. The equations of motion of the T-2 are solved for the control deflections which result in the model responses in the following manner.

The force coefficients required for the T-2 to match the model responses are calculated using the force equations given in Appendix A.

$$F = m_{T-2} \left\{ \dot{V}_m + \omega_{x_m} V_m \right\}$$

$$F_{GRAV} = m_{T-2}\, g \begin{bmatrix} -\sin\theta_m \\ \sin\phi_m \cos\theta_m \\ \cos\phi_m \cos\theta_m \end{bmatrix}$$

$$\begin{bmatrix} C_x \\ C_y \\ C_z \end{bmatrix} = \frac{1}{\bar{q}_m S_{T-2}} \left[F - F_{GRAV} \right]$$

The moment coefficients required for the T-2 to match the angular responses of the model are calculated using the moment equations given in Appendix A.

$$M = I_{T-2}\, \dot{\omega}_m + \omega_{x_m} I_{T-2}\, \omega_m$$

$$\begin{bmatrix} C_\ell \\ C_m \\ C_n \end{bmatrix} = \begin{bmatrix} \frac{1}{b_{T-2}} & 0 & 0 \\ 0 & \frac{1}{\bar{c}_{T-2}} & 0 \\ 0 & 0 & \frac{1}{b_{T-2}} \end{bmatrix} \frac{M}{\bar{q}_m S_{T-2}}$$

These moment coefficients are defined at the c.g. of the T-2. The aerodynamics of the T-2 are defined at $.25\bar{c}$. C_m and C_n must be transformed to account for this difference in c.g. position by

$$\Delta CG_{T-2} = CG_{POS_{T-2}} - 0.25$$

$$C_{m_{0.25\bar{c}}} = C_m + C_z \Delta CG_{T-2}$$

$$C_{n_{0.25\bar{c}}} = C_n - C_y \Delta CG_{T-2} \frac{\bar{c}_{T-2}}{b_{T-2}}$$

Knowing $C_{n_{0.25\bar{c}}}$, C_l and C_y the T-2 lateral-directional aerodynamic equations of Appendix B can be solved for the control deflections which achieve them. All state variables in these equations are equated to those of the model. δ_r is solved for first since $C_{n_{0.25\bar{c}}}$ depends only on this control.

$$\delta_r = -\frac{1}{0.000886}\left[C_{n_{0.25\bar{c}}} - 0.0147\left(\frac{\beta_m}{10}\right) + 0.0167\left(\frac{\alpha_m}{10}\right)\frac{p_m}{V_m} + 0.0499\left(\frac{r_m}{V_m}\right)\right]$$

Knowing δ_r the C_l equation can be solved for δ_a.

$$\delta_a = -\frac{1}{0.00319}\left[C_l - \left[-0.0247\left(\frac{\beta_m}{10}\right) + 0.000708\left(\frac{\beta_m}{10}\right)^3\right]\left[1 - 0.0607\left(\frac{\alpha_m}{10}\right)\right] + 0.176\left(\frac{p_m}{V_m}\right) - \left[0.0333 + 0.03886\left(\frac{\alpha_m}{10}\right)\right]\left[\frac{r_m}{V_m}\right] - 0.00223\left(\frac{\delta_r}{10}\right)\right]$$

The C_y equation can then be solved for δ_y. For simplicity the side-force effectiveness coefficient was linearized.

$$\delta_y = \frac{1}{0.015}\left[C_y + 0.149\left(\frac{\beta_m}{10}\right) + 0.00267\left(\frac{\beta_m}{10}\right)^3 - \left[-0.0283 + 0.03054\left(\frac{\alpha_m}{10}\right)\right]\frac{p_m}{V_m} - 0.0183\left(\frac{\delta_r}{10}\right) + 0.150\left(\frac{\beta_m}{10}\right)\right]$$

An incremental value of the control deflection is computed since the initial value of the control deflections computed by the previous equations may not be the same as the trim value due to linear approximations. Therefore,

$$\Delta\delta_a = \delta_a - \delta_a(t_o)$$
$$\Delta\delta_r = \delta_r - \delta_r(t_o)$$
$$\Delta\delta_y = \delta_y - \delta_y(t_o)$$

The command signal is given by the incremental value plus the trim signal.

$$\begin{bmatrix} \delta_{a_c} \\ \delta_{r_c} \\ \delta_{y_c} \end{bmatrix} = \begin{bmatrix} \Delta\delta_a \\ \Delta\delta_r \\ \Delta\delta_y \end{bmatrix} + \begin{bmatrix} \delta_{a_t} \\ \delta_{r_t} \\ \delta_{y_t} \end{bmatrix}$$

The same general approach is used to calculate the longitudinal controls. The C_D and C_L required of the T-2 must be calculated first since the T-2 aerodynamics are expressed in terms of these variables.

$$\begin{bmatrix} C_D \\ C_L \end{bmatrix} = \begin{bmatrix} -\cos\alpha_m & -\sin\alpha_m \\ \sin\alpha_m & -\cos\alpha_m \end{bmatrix} \begin{bmatrix} C_x \\ C_z \end{bmatrix}$$

The variable $C_{L_{U.T.}}$ is then calculated.

$$C_{L_{U.T}} = \left[0.846 - 0.307\,Mn + 0.823\,M^2n\right]\left[1 - 0.0255\left(\frac{\beta_m}{10}\right)^2\right]\left[\frac{\alpha_m}{10}\right]$$

Estimates of the longitudinal controls were solved for using the aerodynamic equations of Appendix B and linearized control effectiveness coefficients. The control coupling present in these equations was taken into account. The result is a set of three equations and three unknowns which have been put in matrix form as follows. All state variables have been equated to those of the model aircraft.

$$\begin{bmatrix} CLDE & CLTC & CLDZ \\ 0 & -1 & CDDZ \\ CMDE & CMTC & CMDZ \end{bmatrix} \begin{bmatrix} \bar{\delta}_e \\ \bar{T}_c' \\ \bar{\delta}_z \end{bmatrix} = \begin{bmatrix} CL \\ CD \\ CM \end{bmatrix}$$

where the matrix entries are defined as

$$CLDE = 0.1\left[0.086 - 0.0224\left(1 + 1.67e^{-\frac{h_m}{27180}}\right) Mn_m^2\right]$$

$$CMDE = -0.0276\left[1 - 0.233\left(1 + 1.76e^{-\frac{h_m}{28000}}\right) Mn_m^2\right]$$

$$CLTC = 0.0525 + 0.241\left(\frac{\alpha_m}{10}\right)$$

$$CMTC = 0.21 + 0.104\left(\frac{\alpha_m}{10}\right)$$

$$CLDZ = 0.0209$$

$$CDDZ = 0.00216\left[K_{DDZ} + 0.7329\left(\frac{\alpha_m}{10}\right)\right]$$

K_{DDZ} = 1. if previous $\delta_z \geq 0$
= -1. if previous $\delta_z < 0$

K_{DDZ} arises from the linearization of $|\delta_z|$ present in the drag equation of Appendix B.

$$CMDZ = 0.1\left[-0.004 + 0.0142\left(\frac{\alpha_m}{10}\right)\right]$$

$$CL = C_L - C_{L_{U.T.}} - K_{L.G._{T-2}}\left[-0.045 + 0.0375\left(\frac{\alpha_m}{10}\right)\right]$$

$$CD = C_D - 0.02 - 0.0798\, C_{L_{U.T.}}^2 - K_{L.G._{T-2}}\left[0.031 - 0.005\left(\frac{\alpha_m}{10}\right)^2\right] - 0.01\left(\frac{\delta_y - \beta_m}{10}\right)^2$$

$$CM = C_{m_{0.25\bar{c}}} - \left[0.0368 - 0.0364\,Mn_m + 0.0518\,Mn_m^2\right] + 0.004\,K_{L.G._{T-2}}$$
$$- \left[-0.148 + 0.0918\left(1 + 0.756\,e^{-\frac{h_m}{28742}}\right)Mn_m^2\right]\left[1 - 0.03\left(\frac{\beta_m}{10}\right)^2\right]\left[\frac{\alpha_m}{10}\right]$$
$$- \left[-0.693 + 0.131\,Mn_m - 0.407\,Mn_m^2\right]\left[\frac{q_m}{V_m}\right]$$
$$- \left[-0.236 - 0.2947\,Mn_m^2\right]\left[\frac{\alpha_m}{V_m}\right]$$

A better estimate of δ_z is obtained by solving the lift equation taking into account the nonlinear effectiveness of δ_z and $\bar{\delta}_e$ and $\bar{T}_c'$.

$$-0.00315\left(\frac{\delta_z}{10}\right)^3 + 0.209\left(\frac{\delta_z}{10}\right) + \left[-CL + CLDE\,\bar{\delta}_e + CLTC\,\bar{T}_c'\right] = 0 \qquad \text{(E.1)}$$

The drag equation is solved for a better estimate of T_c' knowing δ_z and $\bar{\delta}_e$.

$$T_c' = -CD + \left[0.0216\left|\frac{\delta_z}{10}\right| + 0.01583\left(\frac{\alpha_m}{10}\right)\left(\frac{\delta_z}{10}\right) + 0.00112\left(\frac{\delta_z}{10}\right)^2\right]$$

A better estimate of δ_e is obtained by solving the pitching moment equation taking into account the nonlinear effectiveness of δ_e and the values of T_c' and δ_z just calculated. The equation used is

$$\left[0.0226\left(\frac{\delta_e}{10}\right)^3 - 0.276\left(\frac{\delta_e}{10}\right)\right]\left[CMDE\right]\left[\frac{10}{-0.276}\right]$$
$$+ \left[-CM + CMDC\,\delta_z + CMTC\,T_c'\right] = 0 \qquad \text{(E.2)}$$

The thrust is obtained from

$$T = T_c'\,\bar{q}\,\delta_{T-2}$$

An incremental value of the control deflection is computed since the initial value of the controls computed by the previous equations may differ from the trim values due to approximations.

$$\Delta\delta_e = \delta_e - \delta_e(t_o)$$

$$\Delta T = T - T(t_o)$$

$$\Delta\delta_z = \delta_z - \delta_z(t_o)$$

The command signal is then given by

$$\begin{bmatrix} \delta_{e_c} \\ T_c \\ \delta_{z_c} \end{bmatrix} = \begin{bmatrix} \Delta\delta_e \\ \Delta T \\ \Delta\delta_z \end{bmatrix} + \begin{bmatrix} \delta_{e_t} \\ T_t \\ \delta_{z_t} \end{bmatrix}$$

Further consideration is now given to the algorithm used to calculate δ_e and δ_z when their nonlinear effectiveness is taken into account. As discussed previously, the effectiveness of each surface is cubic in nature. Therefore, three possible control deflections exist and the computer must select the proper one. The method programmed for doing this is now discussed.

The equation from which δ_e or δ_z is calculated is of the form $f(\delta) = A\delta^3 + B\delta + C$. For example, δ_z is calculated from Equation (E.1), the lift equation, and δ_e from Equation (E.2), the pitching moment equation. C varies with α, the lift or pitching moment which must be generated, landing gear position, etc. A plot of $f(\delta)$ vs. δ for three values of C is shown in Figure E.1. Also shown is a curve generated using the linearized surface effectiveness.

Real roots of $f(\delta)$ exist at the intersection of the horizontal axis and the $f(\delta)$ curve. When $C = C_1$, there are three real solutions to the cubic equation or three values of the control deflection which satisfy the equation $f(\delta) = 0$. One negative real root and a complex pair exist when $C = C_2$ while a complex pair and one positive real root exist when $C = C_3$. δ_P and δ_N are defined as the control deflections at the local maximum and minimum of $f(\delta)$. When three real solutions of $f(\delta)$ exist one must be

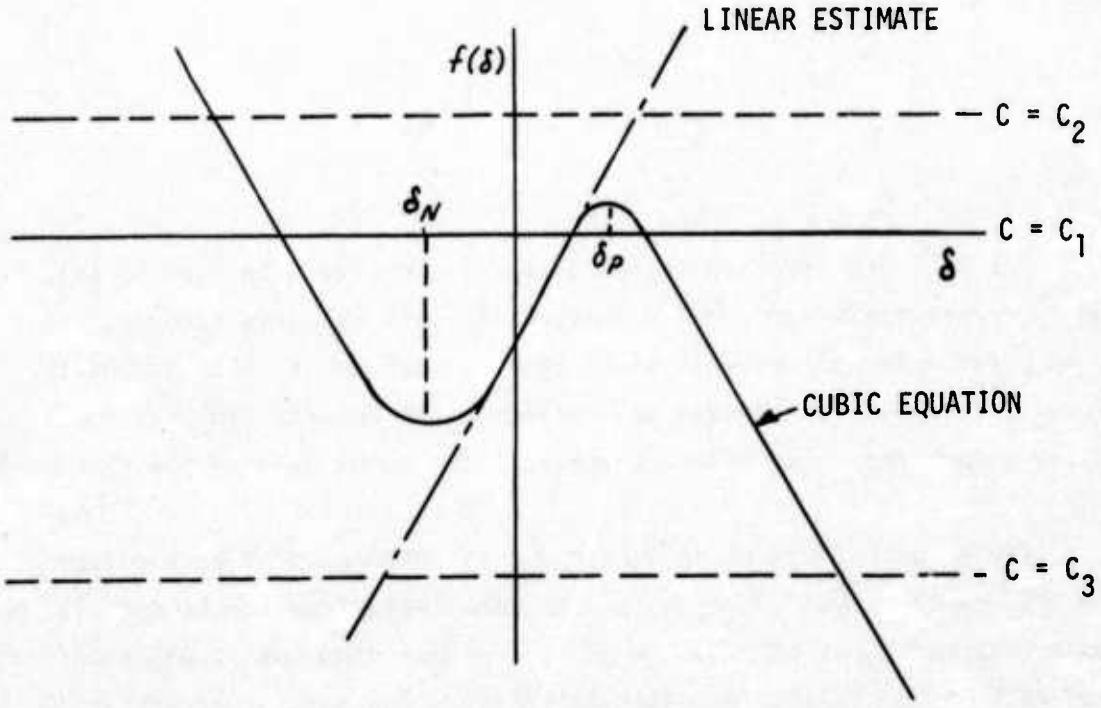

Figure E.1 SKETCH OF NONLINEAR CONTROL EFFECTIVENESS

between δ_P and δ_N . This is the value chosen for the control deflection. When C is such that a positive control deflection larger than δ_P is obtained e.g. $C = C_3$. The control deflection is set at δ_N . This is done because the linearized estimated of the control deflection indicates that large negative value of δ is required and δ_N is the most effective value. The opposite approach is taken when the coefficient C is such that a negative control deflection larger than δ_N is obtained.